Journal of Pharmaceutical Sciences 000 (2023) 1–12

Contents lists available at ScienceDirect

Journal of Pharmaceutical Sciences

journal homepage: www.jpharmsci.org

Pharmaceutics, Drug Delivery and Pharmaceutical Technology

Precise Fabrication of Ocular Inserts Using an Innovative Laser-Driven CaliCut Technology: *In Vitro* and *in Vivo* Evaluation

Dhwani Rana[a], Jayesh Beladiya[b], Devang Sheth[b], Sagar Salave[a], Amit Sharma[a], Anil B. Jindal[c], Rikin Patel[d], Derajram Benival[a,*]

[a] *Department of Pharmaceutics, National Institute of Pharmaceutical Education and Research -Ahmedabad (NIPER-A), India*
[b] *Department of Pharmacology, L.M. College of Pharmacy, Ahmedabad, India*
[c] *Department of Pharmacy, Birla Institute of Technology and Science Pilani (BITS PILANI), Pilani Campus, Rajasthan, 333031, India*
[d] *Graduate School of Pharmacy, Gujarat Technological University Gandhinagar Campus, Gandhinagar, 382028, India*

ARTICLE INFO

Article history:
Received 13 August 2023
Revised 14 December 2023
Accepted 14 December 2023
Available online xxx

Keywords:
CaliCut
Precision
Ocular inserts
Castor oil
Polymer
Laser
HME

ABSTRACT

Ocular inserts offer distinct advantages, including a preservative-free drug delivery system, the ability to provide tailored drug release, and ease of administration. The present research paper delves into the development of an innovative ocular insert using CaliCut technology. Complementing the hot melt extrusion (HME) process, CaliCut, an advanced technology in ocular insert development, employs precision laser gauging to achieve impeccable cutting of inserts with desired dimensions. Its intelligent control over the stretching process through auto feedback-based belt speed adjustment ensures unparalleled accuracy and consistency in dosage form manufacturing. Dry eye disease (DED) poses a significant challenge to ocular health, necessitating innovative approaches to alleviate its symptoms. In this pursuit, castor oil has emerged as a promising therapeutic agent, offering beneficial effects by increasing the thickness of the lipid layer in the tear film, thus improving tear film stability, and reducing tear evaporation. To harness these advantages, this study focuses on the development and comprehensive characterization of castor oil-based ocular inserts. Additionally, *in-vivo* irritancy evaluation in rabbits has been undertaken to assess the inserts' safety and biocompatibility. By harnessing the HME and CaliCut techniques in the formulation process, the study demonstrates their instrumental role in facilitating the successful development of ocular inserts.

Introduction

Dry Eye Disease (DED) is a prevalent ocular surface disorder, impacting millions of people worldwide and ranking as a leading cause for seeking assistance from eye care professionals.[1] DED leads to the instability of the tear film, posing potential harm to the ocular surface. Moreover, it is associated with elevated tear film osmolarity and inflammation of the ocular surface.[2] The incidence of DED is on the rise, and its detrimental effects on vision, work productivity, and overall quality of life are significant.[3,4] With the increasing use of digital devices in our daily lives, a significant portion of the population, including younger generations, faces a higher risk of experiencing digital eye strain and related dry eye symptoms. Managing DED requires chronic therapy. While over-the-counter ocular lubricants and artificial tears remain the primary treatment approaches, they often need to be applied multiple times a day, causing inconvenience for patients.[5] Furthermore, the currently available multi-dose drug products for DED management often contain preservatives. Prolonged use of preservatives in eye drops has been associated with corneal and conjunctival damage, adding to concerns about their long-term use.[6]

Ocular inserts are small, solid, or semi-solid polymeric devices specifically designed for application in the inferior conjunctival sac of the eye. These inserts offer numerous advantages, such as prolonged ocular residence time of the drug, precise dosing, sustained drug release, and reduced frequency of drug administration. These benefits ultimately lead to improved patient compliance with the treatment regimen.[7] Furthermore, ocular inserts are designed to be user-friendly and simple to apply. In cases where patients require long-term therapy, preservative-free inserts are highly recommended. The absence of preservatives reduces the risk of side effects, making them a safer and more suitable option for managing DED and related conditions over an extended period. Lacrisert is an ocular insert approved by the United States Food and Drug Administration (USFDA) for the

* Corresponding author at: National Institute of Pharmaceutical Education and Research - Ahmedabad (NIPER-A) An Institute of National Importance, Government of India, Department of Pharmaceuticals, Ministry of Chemicals and Fertilizers, Opp. Airforce Station, Palaj, Gandhinagar, 382355, Gujarat, India.
E-mail address: derajram@niperahm.res.in (D. Benival).

https://doi.org/10.1016/j.xphs.2023.12.015
0022-3549/

management of DED, comprising hydroxypropyl cellulose (HPC) as its sole active ingredient.[8]

Hot melt extrusion (HME) is a continuous pharmaceutical manufacturing process that is widely employed for the manufacturing of inserts/implants. Employing HME in pharmaceutical insert production demands exceptional precision during the post-extrusion phase of the polymeric blend. The cutting of the insert is a critical step, and the quality of the cutting surfaces depends significantly on the precise combination of the polymer formulation and the chosen cutting method.[9]

The CaliCut™ post-extrusion system provides precise calibration of polymer strands and cutting into well-defined inserts of desired dimensions. This next-generation modular instrument is used in the production of ocular inserts.[10] Combining HME with CaliCut facilitates the fabrication of ocular dosage forms with the desired dimensions. The advancements in equipment allow for an extremely cost-effective formulation of ocular inserts compared to conventional eye drops. Hence, the primary objective of this study is to investigate the potential of CaliCut in combination with HME for developing innovative castor oil-loaded HPC-based ocular inserts for the chronic management of DED. The utilization of HPC in Lacrisert® lends support to the proposition of employing HPC for our current application. However, it is worth noting that Lacrisert exclusively comprises HPC as its active ingredient and does not incorporate castor oil. Nonetheless, the enhancement of treatment potential can be achieved by introducing additional beneficial ingredients. In our proposal, we aim to build upon this foundation by introducing castor oil as an additional component in the ocular insert. This innovation is driven by the potential benefits that castor oil can offer in enhancing the treatment of dry eye conditions. The research focuses on thoroughly characterizing these novel ocular inserts to evaluate their properties and performance. Notably, this study is groundbreaking, being the first of its kind to utilize CaliCut as a post-extrusion system in the development of ocular inserts, adding a pioneering dimension to the investigation.

Materials and Methods

Materials

Hydroxy propyl cellulose (HPC) [Klucel™- HXF grade, MW 1150 kDa], castor oil, and dexamethasone were obtained as a gift sample from Ashland, India; Croda, India; and Cadila Pharmaceuticals Ltd., India, respectively. Sodium chloride, potassium chloride, potassium dihydrogen orthophosphate, anhydrous di-sodium hydrogen orthophosphate, and anhydrous calcium chloride were procured from Qualigens, Thermo Fisher Scientific India Pvt. Ltd. Acetonitrile (ACN) utilized was of high-performance liquid chromatography (HPLC) grade, sourced from Thermo Fisher Scientific, India. Ultrapure (Milli Q) water from the Merck Millipore system was used throughout the investigation. All other chemicals used in the study were of analytical grade.

Preparation of Ocular inserts

The inserts were prepared using HME, followed by CaliCut. First, a mixture of castor oil (20% w/w) and the polymer HPC (Klucel™) (80% w/w) was thoroughly mixed. This physical blend was then fed into a co-rotating twin-screw extruder (Haake™ Mini CTW Micro-Conical Twin Screw Compounder, Thermo Fisher Scientific) at a constant rate. The screw speed during the extrusion process was set at 50 rpm. The extrusion was carried out at a process temperature of 170 °C, and the resulting material was extruded through a 1.5 mm diameter die to form the extrudates.

In order to address the analytical challenges associated with the quantification of castor oil, a different approach was undertaken to determine the drug content and drug release from the inserts. Instead of using plain castor oil, dexamethasone was dissolved in castor oil to obtain a dexamethasone-loaded castor oil solution. This solution was then used in the preparation of inserts with HPC while keeping all other process parameters the same. The rationale behind this approach was to utilize dexamethasone as a surrogate for the analysis of castor oil. Dexamethasone is a lipophilic compound that readily dissolves in castor oil. Moreover, it possesses a strong chromophore that allows its detection using HPLC and diode array detector. By using dexamethasone-loaded castor oil instead of plain castor oil, it becomes possible to quantify the drug content and track the drug release from the inserts through the analysis of dexamethasone using HPLC. This strategy simplifies the analysis and provides a reliable means of evaluating the inserts' characteristics. Additionally, comprehensive studies involving Thermogravimetric Analysis (TGA), Differential Scanning Calorimetry (DSC), Attenuated Total Reflectance Fourier Transform Infrared spectroscopy (ATR-FTIR), and Raman analysis were conducted on inserts loaded with dexamethasone.

Post-Extrusion Processing Using CaliCut

The CaliCut post-extrusion system (Citius, Thermo Fisher Scientific) was utilized for the precise cutting of the extrudates in order to attain the desired dimensions, i.e., diameter and length. The diameter gauge positioned at the inlet of the CaliCut measures the diameter of the extrudate and accordingly controls its stretching by providing auto feedback to conveyor belt speed as the extrudate is pulled towards the cutter (The authors have not had any previous or present financial involvement, support, engagement, or endorsement in research related to CaliCut or Thermo Fisher Scientific). The extent of stretching depends on the diameter of the extrudate that is coming out of the die of the HME. Therefore, it is self-evident that if the desired diameter of the insert/implant is 0.5 mm, then the die to be used in HME should be $\geq$ 0.5 mm so that effective stretching can be applied for precise control of the set diameter. In addition, the effective guiding and driving of the extrudate are guaranteed by freewheel rollers. Hence, the extrudates from the die were simultaneously stretched at the belt speed set by the machine as per the desired diameter and then subjected to cutting. Since different polymeric materials may behave differently during the cutting process, which can affect the surface finish of the insert/implant, CaliCut also has heating provision to control the temperature of the extrudates. The cutting device cuts the stretched polymeric extrudate by pushing the cutting blade forward through the lever to the desired length. For our ocular insert, the nominal diameter and length were set at 1.30 mm and 3.50 mm, respectively. Accordingly, the tolerance values for the minimum and maximum diameter were set at 1.25 and 1.35 mm, respectively. Similarly, the tolerance values for the minimum and maximum length of inserts were set at 3.45 mm and 3.55 mm, respectively.

It is imperative to acknowledge that the effectiveness of any manufacturing process depends on various factors, including the specific materials used, the design of the machinery, and the intended application. The CaliCut makes the manufacturing process continuous, unlike injection molding, which is a batch process. This enhances productivity enormously in a production environment. The surface finish is primarily governed by the extruder, and exploiting the heating provision of CaliCut aids in achieving smooth edges of inserts, which is important from the biocompatibility (local tissue irritation) perspective. Since the screw extruder design is conical, which leads to a very high pressure and therefore ensures that the flow is regulated, the implants are very uniform and devoid of sharp edges.

HPLC Chromatographic Conditions

The analysis of dexamethasone was conducted using an HPLC system from Agilent (1260 infinity II). For the chromatographic separation, an Agilent Eclipse Plus C18 column with particle size 5 μm and dimensions 4.6 $\times$ 250 mm was utilized. The mobile phase composition consisted of Milli Q water as the aqueous phase (A) and ACN as the organic phase (B). A gradient program was employed for the separation, with the following time (mins) and corresponding % of phase A (%A): 0/60, 1/60, 2/40, 4/40, 6/60, and 7/60. The flow rate was adjusted at 1.2 ml/min. For each analysis, an injection volume of 30 μl was used, and the diode array detector was set to a wavelength of 241 nm for detection. The total run time was set at 7 mins in gradient mode. Data acquisition and analysis were performed using the Openlab software.

Evaluation of Ocular Insert

The castor oil-loaded inserts prepared using HME and CaliCut underwent a comprehensive evaluation to assess various parameters. These included appearance, dimensions (diameter and length), weight variation, surface pH, swelling index, drug content, percentage moisture absorption, percentage moisture loss, mechanical properties, *in vitro* drug release, and *in vivo* irritancy.

Dimensional Analysis and Uniformity of Weight

Inserts (n = 100) were chosen at random and weighed individually with a digital balance (Mettler Toledo). The inserts' average weight was calculated. A digital vernier caliper (General Ultratech) was used to measure the dimensions of the inserts. One hundred inserts were chosen at random for measurement of length and diameter, and their respective means were recorded.[11]

Drug Content

To assess the uniformity of content, ocular inserts (n = 10) were individually weighed and dissolved in methanol.[12] The resulting solubilized samples were subsequently analysed using HPLC at a wavelength of 241 nm, allowing for the quantification of dexamethasone content in each insert. This comprehensive analysis also facilitated the evaluation of content uniformity, ensuring consistent drug distribution throughout all the inserts.

Surface pH

The surface pH of the inserts was assessed by a method involving the swelling of the inserts in a closed Petri dish at room temperature for a duration of 30 mins. During this process, the inserts were exposed to 0.1 ml of distilled water. After the swelling period, the inserts were taken out of the Petri dish and placed on pH paper for surface pH measurement. The inserts were in contact with the pH paper for 60 seconds, allowing the colour to develop. The resulting colour was then compared with a standard colour scale to determine the corresponding pH value.[13–15]

ATR-FTIR and Raman Spectroscopy

The ATR-FTIR spectra of castor oil; HPC; dexamethasone; physical mixture of castor oil, HPC, and dexamethasone; and ocular insert containing all these components were obtained using a Bruker ATR (Alpha opus 7.5).[16] The measurements were carried out at ambient temperature, scanning the range of 4000–600 cm^{-1}. Similarly, Raman spectroscopy measurements were carried out using Raman spectrometer (Horiba Scientific). The analysis was performed at ambient temperature, scanning the range of 4000–400 cm^{-1}. FTIR and Raman analysis were conducted to investigate any molecular interactions between the components in the developed inserts.

TGA

TGA was conducted on castor oil; HPC; dexamethasone; physical mixture of castor oil, HPC, and dexamethasone; and ocular insert containing all these components to assess their thermal stability before and after processing them to HME using a Netzsch Thermal Gravimetric Analyzer (TGA 209 F3 Tarsus). The starting materials were weighed at approximately 5–10 mg. The samples were subjected to heating from 30 °C to 450 °C at a heating rate of 10 °C/min under nitrogen flow.[17] This gradual increase in temperature allowed for the observation of any weight loss or decomposition events that occurred as the materials were heated.

DSC

DSC analysis of HPC; dexamethasone; physical mixture of castor oil, HPC, and dexamethasone; and ocular insert containing all these components were performed using a DSC-60 Plus (Shimadzu). Each sample, consisting of approximately 5–10 mg, was securely sealed in standard aluminium pans. The temperature analysis ranged from 30 to 300 °C, with a heating rate of 10 °C/min, and a continuous nitrogen purging at a rate of 50 ml/min was maintained throughout the experiments.[18,19]

Swelling Index

The swelling index of the ocular inserts was established by first weighing each insert and then immersing it in a glass vial containing phosphate-buffered saline (PBS) with a pH of 7.4. At specific time intervals (5, 10, 15, 30, 45, and 60 min) during the experiment, the inserts were removed from the PBS solution. Any excess liquid was carefully removed by gently wiping the insert using filter paper, then weighed again. The swelling index was calculated for three ocular inserts chosen at random using Equation 1.[20] Moreover, changes in the dimensions of the inserts were monitored at various time points to precisely evaluate swelling and alterations in size.

$$\textit{Swelling index}\ (\%) = \frac{\textit{Weight of swollen insert}\ (mg) - \textit{Initial weight of insert}\ (mg)}{\textit{Initial weight of insert}\ (mg)} \times 100 \quad (1)$$

Percentage Moisture Absorption

The integrity of the inserts was assessed through a moisture absorption test, where the percentage of moisture absorption was determined. Inserts (n = 3) were weighed individually and kept inside a desiccator maintained at high relative humidity (RH), housing a saturated solution of sodium chloride to maintain a high RH (approximately 75 % RH). The desiccator was sealed for three days, and the humidity level inside the desiccator was monitored using a digital humidity meter (Traceable, Fisher Scientific). After the designated three-day duration, the inserts were carefully taken out of the desiccator and weighed again to determine their final weight.[21,22] Equation 2 was applied to analyse the percentage of moisture absorption.

$$\%\ \textit{Moisture absorption} = \frac{\textit{Final weight of insert}\ (mg) - \textit{Initial weight of insert}\ (mg)}{\textit{Initial weight of insert}\ (mg)} \times 100 \quad (2)$$

Percentage Moisture Loss

The stability of the inserts under dry conditions was assessed by conducting a percentage moisture loss analysis. Three inserts were weighed individually and kept inside a desiccator that contained anhydrous calcium chloride. The humidity level within the desiccator was monitored using a digital humidity meter (Traceable, Fisher Scientific). The inserts were removed from the desiccator after three days and weighed once again to ascertain their final weight. Subsequently, the percentage of moisture loss was determined by employing Equation 3.[22]

$$\%\ Moisture\ loss = \frac{Initial\ weight\ of\ insert\ (mg) - Final\ weight\ of\ insert\ (mg)}{Initial\ weight\ of\ insert\ (mg)} \times 100 \quad (3)$$

Mechanical Properties

The mechanical properties of ocular inserts, namely, tensile strength and percent elongation, were assessed to determine their resistance to breaking caused by the blinking action of the eye.[23] This evaluation was conducted using a Universal Testing Machine (H5KT, Tinius Olsen) with a 50 N load cell at a temperature of 25 °C. The ocular inserts (n = 3), with dimensions of 1.3 mm × 30 mm, were securely clamped between two fixtures placed 10 mm apart. They were then pulled at a rate of 5 mm/min until they tore, allowing for the measurement of their tensile strength and percent elongation.[24]

Optical Microscopy and Field Emission Scanning Electron Microscopy (FE-SEM)

The morphology of the fabricated inserts was examined using optical microscopy (Leica ICC50 E) and FE-SEM (Zeiss Sigma 300, Germany). For the optical microscopy analysis, the samples were directly observed by placing them on a slide and examining them under the microscope. No additional sample preparation techniques were employed. Further, for SEM analysis, to prepare the samples for examination, the inserts were securely placed on a metal stand using conductive adhesive tape. Prior to imaging, a thin layer of gold coating was applied to the samples in an inert atmosphere. The gold coating process involved applying a current of 10 mA for a duration of 60 seconds.[25,26] Moreover, the surface topography was determined, and 3D surface image was captured.

In Vitro *Drug Release Study*

The *in vitro* release study was conducted using an assembly consisting of a 10 ml beaker and a mesh. The insert was positioned inside a glass beaker containing PBS (pH 7.4) as the release medium. The selection of the release media was determined by the solubility of dexamethasone in PBS, which was found to be 133.31 ± 0.09 μg/ml. Notably, the solubility of dexamethasone far exceeded the required levels to maintain sink conditions, as each insert contained 5.35 μg of dexamethasone dissolved in castor oil, whereas 5 ml of release media was used. Here, it can further be noted that the solubility of dexamethasone in castor oil was calculated to be 11.57 ± 0.19 mg/ml.[27] Each insert contained 1.042 μl of castor oil (20% w/w), and within this castor oil, 5.35 μg of dexamethasone was dissolved. It is worth noting that, as per the obtained solubility of dexamethasone in castor oil, this allows for a maximum incorporation of 12.05 μg of dexamethasone into 1.042 μl of castor oil. The ocular insert was positioned in a glass beaker covered with a mesh; a stir bar was positioned on top of the mesh; and the release medium was added to the beaker.[7] The entire setup, including the beaker, insert, mesh, and stir bar, was placed on a multi-station hot plate (IKA RT 10) maintained at a temperature of 34 ± 0.2 °C. Continuous stirring was applied and samples were collected at predetermined time intervals of 0.25, 0.5, 1, 3, 6, 9, 12, and 15 h. The obtained aliquots were subjected to HPLC for quantification of dexamethasone. The release data was plotted, correlating the amount of dexamethasone released from the inserts with the corresponding time points. The study was conducted in triplicate, and the obtained results are displayed as the mean ± SD.

Determination of Drug Release Kinetics

For gaining deeper insights into the mechanisms underlying the release of drug from polymeric matrices, the *in vitro* release data of the ocular inserts were analysed (DDSolver software). Various kinetic models, namely Zero-order, First-order, Higuchi, Korsmeyer-Peppas, and Hixson-Crowell, were employed to analyse the release data. The results obtained from this analysis were assessed based on statistical parameters such as adjusted coefficient of determination (R^2), Akaike Information Criterion (AIC), and Model Selection Criterion (MSC). The model exhibiting the highest correlation was selected to describe the primary release mechanism.[20,28]

In Vivo *Eye Irritancy Test*

The ocular irritation potential of the developed inserts was assessed by the Draize eye irritancy test. This test evaluates the ability of the inserts to cause harm to the cornea, iris, and conjunctiva upon application to the eye.[22] Prior to the test, the inserts underwent sterilization using UV radiation. The study protocol received approval from the Institutional Animal Ethics Committee of L.M. College of Pharmacy, India (LMCP/IAEC/23-01/0074). For the eye irritancy test, adult albino rabbits weighing approximately 2.5 to 3.5 kg of either sex were used. The eye irritation potential of the insert was evaluated using three rabbits as test subjects.[29] Once the lower lid was carefully pulled from the eyeball, the insert was then placed into the conjunctival sac of one eye for each rabbit. The lids were then carefully held together for a few seconds to ensure the insert remained in place. The other eye of the rabbits remained untreated and served as a control. Throughout the study, the test animals were regularly examined to observe any signs of irritation. The evaluation of eye irritation followed the guidelines set by the Organisation for Economic Co-operation and Development (OECD) Test No. 405: Acute Eye Irritation/Corrosion guidelines, which employs a grading system to assess the condition of the cornea, iris, conjunctiva, and chemosis.[30] For the cornea, grades range from 0 (normal), 1 (scattered areas of opacity, where details of the iris remain clearly visible), 2 (easily discernible translucent area, albeit with slightly obscured iris details), 3 (nacrous area, rendering iris details invisible), to 4 (opaque cornea). The iris is graded on its reaction to light and its condition. Grade 0 signifies a healthy state, Grade 1 indicates a reactive response to light, and Grade 2 highlights more severe conditions. Conjunctiva grades go from 0 (normal), 1 (slight hyperemia), 2 (crimson colour), to 3 (distinct beefy red colour). Chemosis, or conjunctival swelling, ranges from 0 (normal), 1 (some swelling above normal), 2 (swelling with partial eversion of lids), 3 (swelling with lids about half closed), to 4 (swelling with lids more than half closed). This comprehensive grading system aids in evaluating the severity of eye conditions based on a range of observable features across these different components. Ocular reactions, specifically the grades of conjunctival, corneal, and iris reactions, were assessed at 1, 24, 48, and 72 h after the instillation of the inserts.

Results and Discussion

Preparation of Ocular Inserts

The preparation of castor oil-loaded inserts was successfully accomplished using a continuous HME process in combination with CaliCut. Castor oil has the ability to complement insufficient physiological tear film lipids, leading to improved lipid spreading properties and a reduction in the evaporation of aqueous tears. Castor oil is expected to render the tears more stable and decrease friction between the ocular surface and eyelid. Research studies have demonstrated that when applied topically to the ocular surface, castor oil exhibits a prolonged residence time. This enhances the thickness and stability of the tear film lipid layer, resulting in the alleviation of associated symptoms.[31] Goto et al. documented the beneficial effects of castor oil in treating ocular surface disorders with meibomian gland dysfunction (MGD). Low-concentration castor oil eye drops have been developed to effectively treat patients suffering from noninflamed obstructive MGD, a significant contributor to lipid-deficiency dry eye. Findings suggested stabilization of tears over the ocular surface and exhibited a uniform pattern of spreading, indicating consistent coverage across the ocular surface.[32] Castor oil eyedrops, developed by Maïssa et al., achieved a residence time of at least 4 h after instillation, resulting in a more stable tear film. This prolonged stability led to a significant reduction in ocular symptoms throughout the entire follow-up period for the individuals experiencing symptoms.[33] Thus, castor oil topical application may offer a safe, natural, economical, and efficient solution for managing common tear film and ocular surface abnormalities, warranting further exploration. Additionally, HPC was selected as the matrix material for the inserts. HPC offers several advantages in ocular applications, including its biocompatibility with ocular tissues, biodegradable nature, and potential for managing DED. HPC, apart from possessing the potential to be used in the management of DED, has shown sufficient thermoplastic characteristics and has been explored for the HME process.[34,11] During the HME process, various parameters, like temperature and screw speed, were optimized to investigate their impact on the extrudability of the inserts. The goal was to ensure smooth and consistent extrusion of the material.

In the case of CaliCut, the extrudate that emerges from the die of the HME (Fig. 1A) is constantly measured for its diameter using a line laser positioned at the machine's inlet (Fig. 1B, 1C). This diameter measurement assists in controlling the belt speed and facilitating the stretching of the extrudate (Fig. 1B(ii)). Additionally, the belt speed can be manually adjusted to meet specific requirements. During this study, to achieve the desired diameter of the inserts within specified tolerances, the system was operated in an automated mode. Laser measurements were used to guide the adjustments of the belt speed, ensuring precise control over the stretching of the extruded strand and enabling accurate diameter adjustments. The stretched extrudate, guided by two efficient freewheel rollers, is conveyed to the cutter. The transparent cover ensures that the extrudate is thermally enclosed, maintaining its consistency for the cutting process. The software allows for configuring the temperature of the heater. For this study, the heating temperature of the stretching and cutting machine was optimized at 55 °C to achieve inserts with smooth

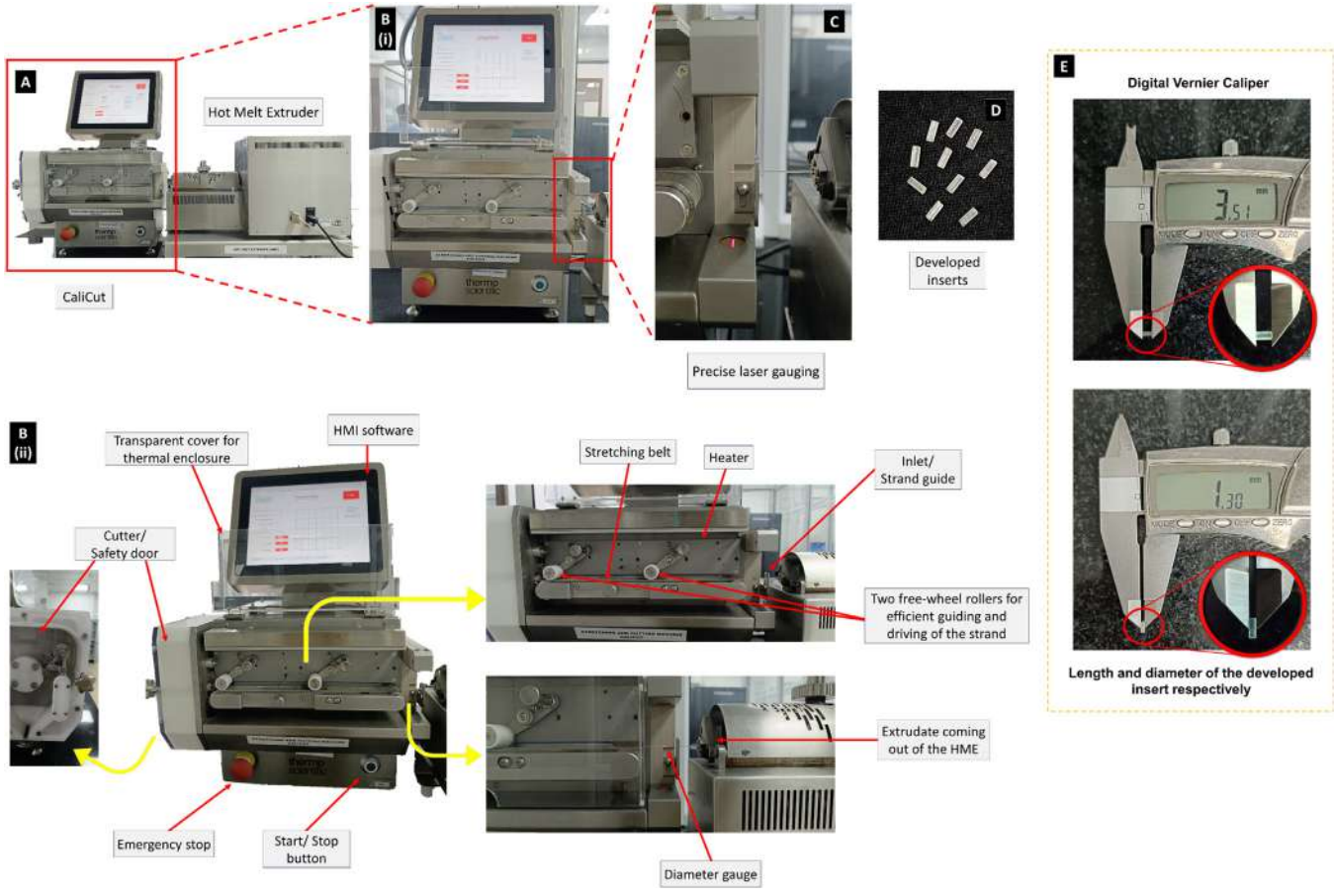

Figure 1. Visual representation of (A) Extrudate coming out of the die of HME, (B, i) Stretching by CaliCut with precise measurement of diameter using laser, (B, ii) Technological stratification of CaliCut, (C) Laser guided measurement of diameter of the extrudate, (D) Oil-loaded inserts obtained from HME and CaliCut, and (E) Analysed length and diameter of the developed insert.

edges. The process concludes with the collection of inserts that have been cut by the CaliCut, following their transition from the belt to the cutter. Fig. 1(A-E) provides a visual representation of the entire process involved in the preparation of ocular inserts, including specific details of the CaliCut process and its relevant parts.

Since CaliCut relies on laser measurements and belt speed adjustments to control the stretching and cutting of the extrudate, having well-defined dimensions (Fig. 1E) ensures that the inserts meet the specified tolerances. When the inserts have consistent dimensions, it allows for better control over the cutting process, resulting in uniform and accurately sized inserts. The success of the CaliCut system is contingent upon the inserts having well-defined dimensions with smooth edges and desired surface characteristics, as this directly influences the precision, quality, and performance of the ocular inserts.

Physical Appearance, Dimensional Analysis, Uniformity of Weight, and Drug Content

The HME and CaliCut techniques resulted in the production of uniformly shaped inserts (Fig. 1D, E). All the developed ocular inserts exhibited a desirable appearance, being semi-transparent and having smooth and consistent surfaces. On average, the inserts weighed around 5 mg and had dimensions of 1.30 mm (diameter) × 3.50 mm (length). The specific dimensions could be influenced by factors such as the temperature used for extrusion, the pressure applied by the die during the extrusion process, and the speed at which the extrudates were stretched by the CaliCut belt. Table S1 presents the recorded values for the weight (4.98 ± 0.10 mg), diameter (1.30 ± 0.02 mm), and length (3.50 ± 0.01 mm) of the developed inserts. The drug content (n = 10) was found to be 99.19 ± 1.44 %.

Surface pH

The normal pH of human tears typically falls within the range of 6.5 to 7.6, with an average value of 7.0.[35] The eye globe has the ability to tolerate topically applied dosage forms with pH values ranging from 3.0 to 8.6, contingent on its buffering capacity.[36,37] In the case of the developed inserts, the surface pH was found to be within the favourable range of 6.0 to 8.0, and based on the composition, the inserts have no significant buffer capacity. This indicates that these inserts can be safe for ocular administration without causing any irritation.

ATR-FTIR and Raman Spectroscopy

The ATR-FTIR spectra of castor oil; HPC; dexamethasone; physical mixture of castor oil, HPC, dexamethasone, and insert are shown in Fig. 2A. The ATR-FTIR analysis was conducted to investigate any potential incompatibility between the materials within the inserts. In the ATR-FTIR spectra of castor oil, characteristic stretching vibrations of hydroxyl groups (ricinoleic acid side chains) were observed between 3595 and 3160 cm^{-1} [38], with a specific peak at 3492 cm^{-1} [39,40]. The −C−H stretching for the long alkyl chain[39] (typical triglyceride ester methyl[40]) and the −C−C bond peaks were detected at 2921 cm^{-1} (asymmetrical CH stretching) and 2861 (symmetrical CH stretching) cm^{-1}, respectively.[38] The C=O stretching of the triglyceride ester linkage appeared at 1733 cm^{-1} [41], while the peak at 1457 cm^{-1} corresponded to C=C stretching.[39] For HPC, an absorption band at 3413 cm^{-1} was observed, which corresponded to the hydroxyl group in the pyranose unit of HPC.[42] Absorption bands at 2975 cm^{-1} and 2876 cm^{-1} were attributable to CH stretching vibration, while the peak at 1459 cm^{-1} indicated O−H, C−H bending, and $-CH_2$ deformation.[43] Furthermore, the ATR-FTIR spectra of dexamethasone demonstrated comparability to those reported in the existing literature. Both the physical mixture and the insert exhibited the presence of all the characteristic peaks in their respective ATR-FTIR spectra, suggesting the absence of any physical or chemical interactions between the components present in the formulation. A similar inference was drawn from the Raman spectra analysis (Fig. 2B). In these spectra, distinct peaks corresponding to castor oil, HPC, and dexamethasone were evident.

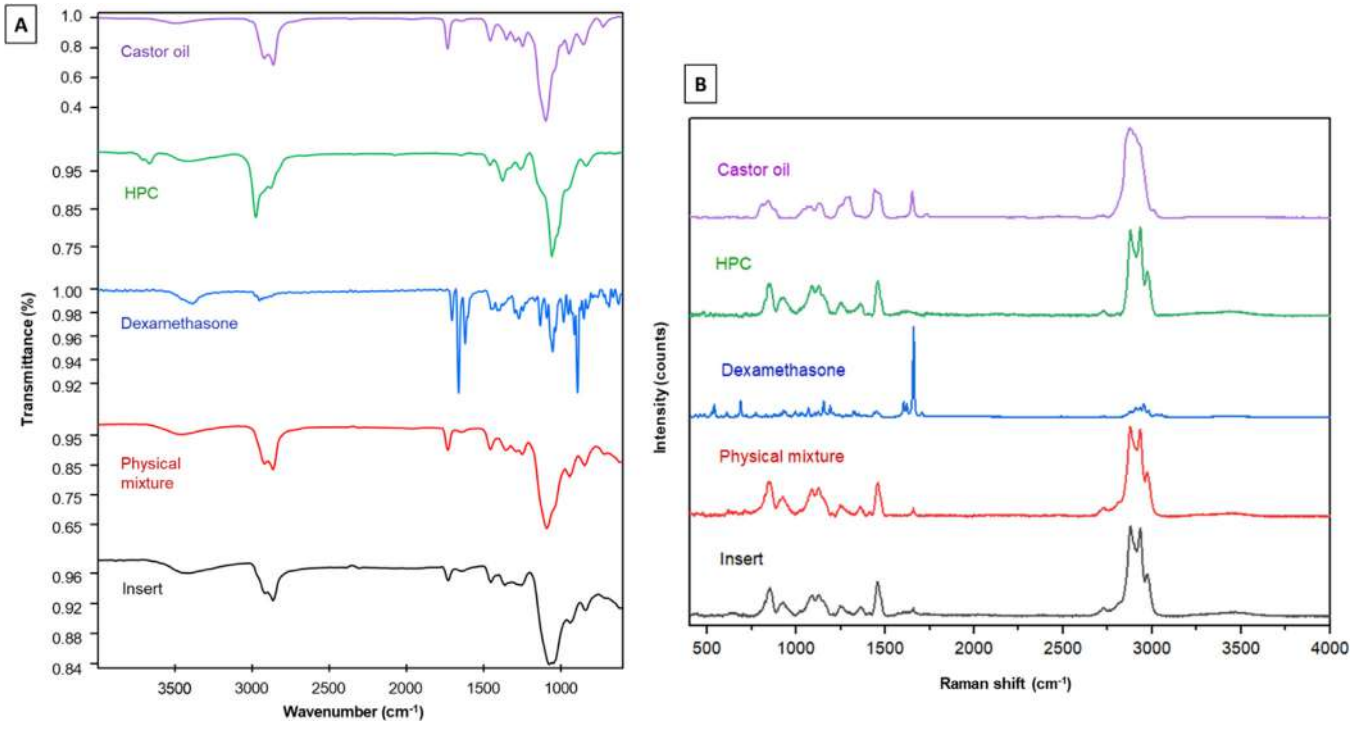

Figure 2. (A) ATR-FTIR spectra of castor oil, HPC, dexamethasone, physical mixture and insert respectively, (B) Raman spectra of castor oil, HPC, dexamethasone, physical mixture and insert respectively.

Conversely, the physical mixture and inserts exhibited similar spectral patterns, with the presence of all characteristic peaks.

TGA

The HME process necessitates heating the polymer and drug to a high temperature. As a result, it is critical to ensure that all of the materials being fed into HME are stable at the processing temperature.[7] The TGA provided valuable insights into the thermal stability characteristics of all the components (i.e., castor oil; HPC; dexamethasone; physical mixture of castor oil, HPC, dexamethasone; and insert). Fig. 3 illustrates that all the formulation components remained sufficiently stable without significant decomposition occurring up to the HME processing temperature of 170 °C used for the insert formulation.

DSC

The thermal characteristics of HPC; dexamethasone; physical mixture of castor oil, HPC, dexamethasone; and insert were investigated using DSC analysis (Fig. 4). Dexamethasone exhibited a distinct endothermic peak at nearly 255 °C, attributed to the melting point of the crystalline drug.[44] HPC did not exhibit any endotherm, aligning with the reported literature.[11,45] The physical mixture did not display the endothermic peak of dexamethasone, potentially suggesting solubilization of the drug within the polymer matrix. Following processing, the characteristic dexamethasone peak was notably absent in the polymeric ocular inserts, signifying the transformation of the drug into an amorphous state during the HME process used for the development of ocular inserts.

Swelling Index

Assessing the swelling index of the insert holds crucial significance as it offers valuable insights into the adhesive properties of the ocular inserts. Polymer swelling is essential in triggering the bioadhesion process, enabling the inserts to adhere to the ocular surface. Essentially, the water-holding ability of the polymers used in the inserts is indicated by the swelling index.[37,46] Fig. 5 depicts the swelling behaviour of the investigated polymeric ocular inserts. Over time, the inserts exhibited an increase in water absorption, primarily due to the hydrophilic nature of the polymer, which creates a gel-like layer when hydrated. Moreover, following exposure to PBS,

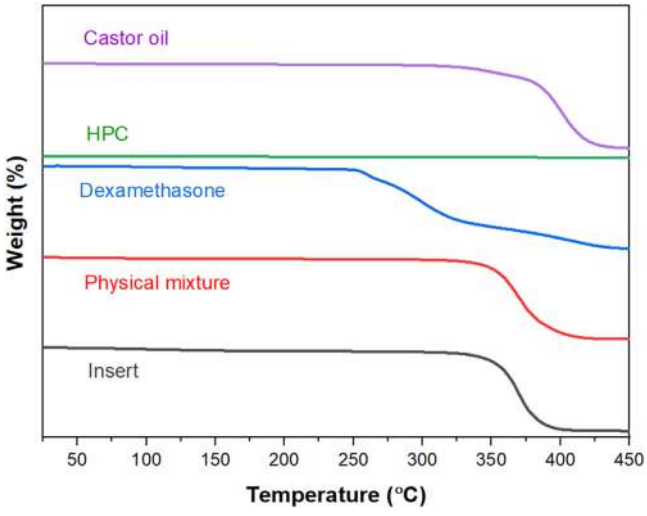

Figure 3. TGA thermograms of castor oil, HPC, dexamethasone, physical mixture and insert.

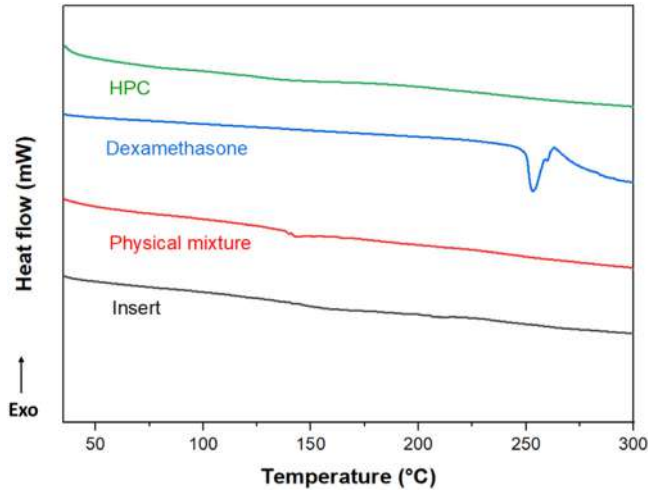

Figure 4. DSC thermograms of HPC, dexamethasone, physical mixture and insert.

noticeable changes in the dimensions of the inserts became apparent. The figure provides a visual representation of the initial insert as well as the changes in dimensions observed at different time points after immersing it in PBS. Observations indicate that the inserts gradually adopt a more spherical shape over time. Ocular inserts adjust in the eye by swelling, which allows them to conform to the eye's contours in such a way that it do not cause any inconvenience. It can be said that upon administration into the eye and leveraging their bioadhesive properties, the inserts would seamlessly adjust as they swell.

Percentage Moisture Absorption and Percentage Moisture Loss

Moisture uptake by solid dosage forms can lead to changes in certain properties, such as increased chemical degradation rates and the risk of microbial contamination.[21] The moisture absorption and loss of inserts were quantified, yielding values of 3.43 % ± 0.24 % and 1.13 % ± 0.19 % respectively (Fig 6). Notably, no change in the integrity of the inserts was observed during the testing conditions of high and low humidity, as determined by their physical appearance. These findings indicate that the ocular inserts exhibit favourable physical stability under both high humidity and dry conditions, emphasizing their suitability for such environments.

Mechanical Properties

The parameters of tensile strength and percentage elongation are indicative of the strength and elasticity of insert.[23] Tensile strength measures the ability of insert to withstand rupture. An ocular insert with good tensile strength can withstand the tearing produced by the blinking action of the eye.[47] The developed inserts exhibited a tensile strength of 21.1 ± 2.48 MPa and a percentage elongation of 50.2 ± 2.33 %, indicating good flexibility and high resistance against breaking. Fig. 7 represents the stress vs strain curve of the developed inserts.

Optical Microscopy and FE-SEM

The morphology of the inserts was assessed employing an optical microscope. Fig. 8(A-D) illustrates the visual representations obtained by the microscope. The inserts exhibited a notably smooth surface texture, devoid of any signs of cracks or structural compromise. The SEM images and 3D surface topography image of the developed insert are shown in Fig. 9(A-D). These visual representations clearly reveal the absence of any sharp edges or rough surfaces on

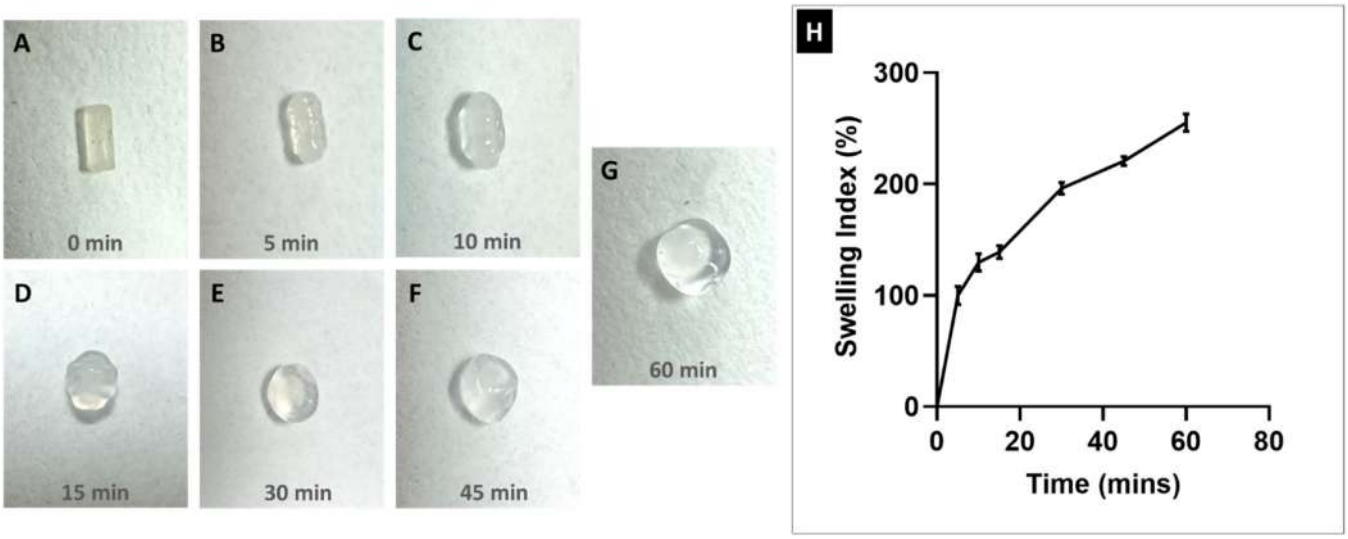

Figure 5. (A-G) Changes in dimensions of inserts with time upon swelling, (H) Swelling index (%) of the developed ocular inserts; mean ± SD (n = 3).

the developed ocular inserts. It is important to emphasize that biocompatibility is not an intrinsic property of a material; rather, it hinges on the biological environment and the specific interactions involving drug-polymer-tissue components.[48] Implants/inserts with smooth surfaces and devoid of sharp edges are generally more biocompatible and trigger less inflammation.[49] Therefore, prioritizing smoother implant/insert designs while avoiding sharp corners that can lead to tissue damage during movement becomes imperative to minimize local tissue damage and the development of chronic foreign body responses.[50] Particularly in the context of ocular inserts, maintaining a smooth surface and edges is of paramount importance. This is crucial to ensure patient acceptance and minimize potential issues.

Through a comprehensive evaluation of all the assessment parameters, a thorough understanding of the inserts' characteristics and performance was achieved.

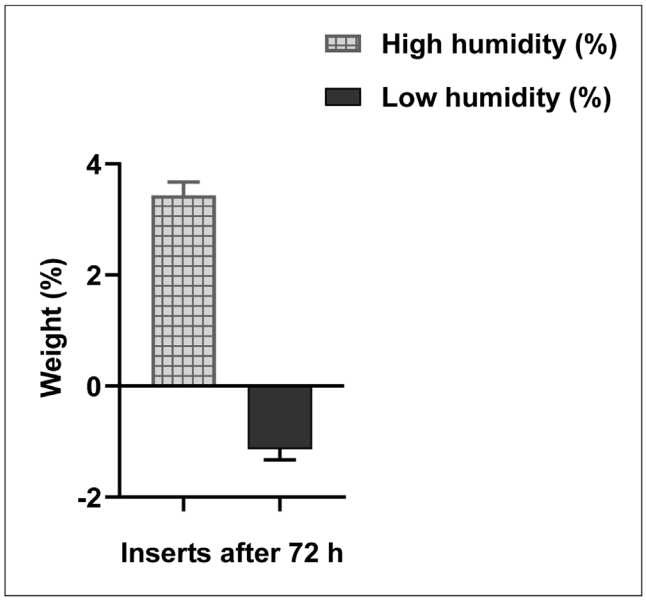

Figure 6. Inserts' weight changes following exposure to low and high humidity environments; mean ± SD (n = 3).

In vitro *Drug Release Study and Drug Release Kinetics*

Upon visual examination, it was observed that the inserts started to hydrate once the release media was introduced into the glass vials above them. The release profile obtained from the *in vitro* release study of the developed ocular insert is graphically illustrated in Fig. 10A. Within 15 h, the drug release reached 92.84 ± 2.54 %.

It is important to emphasize that in this experiment, it is challenging to definitively distinguish between the release of dexamethasone and castor oil. This experiment, however valuable for our purpose, cannot be a perfect discriminator, and it is likely that the release of castor oil and dexamethasone can be different due to differences in their solubilities in an aqueous environment. It is conceivable that dexamethasone may be partitioning from the castor oil into the aqueous phase at a different rate compared to the release of castor oil itself from the HPC insert. It is intuitive to assume that the release of castor oil probably necessitates the erosion of the insert to physically release the oil. However, dexamethasone can potentially enter the receiving medium directly, as its solubility in PBS is below the saturation point. In addition, it is important to note that the attainment of a Zero-order release profile is typically exclusive to planar erodible

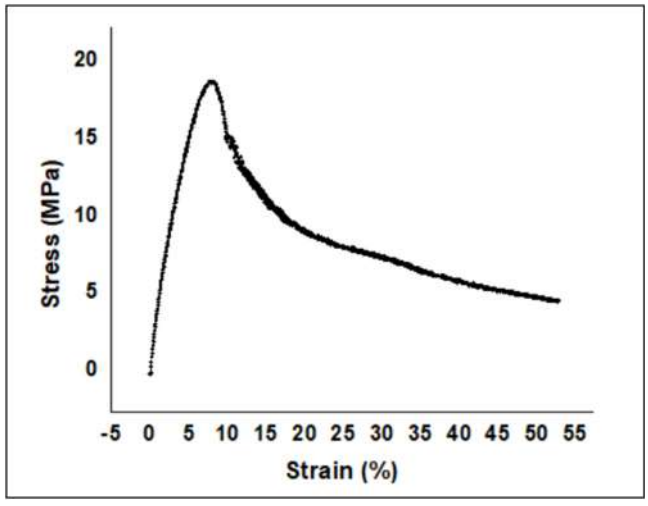

Figure 7. Mechanical strength of the developed insert (stress v/s strain plot).

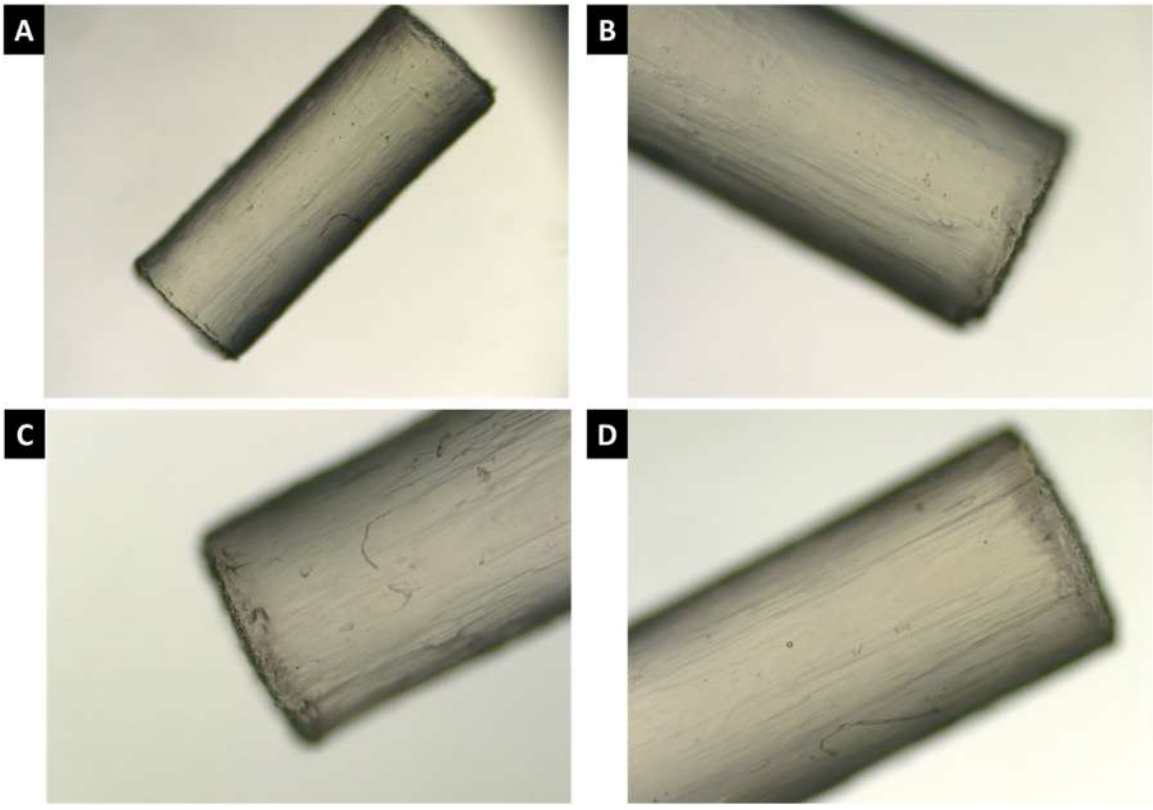

Figure 8. Optical microscopic images of the developed inserts (A) Entire insert (magnification: 2.5 ×) (B), (C) and (D) Surface and edges of inserts (magnification: 4 ×).

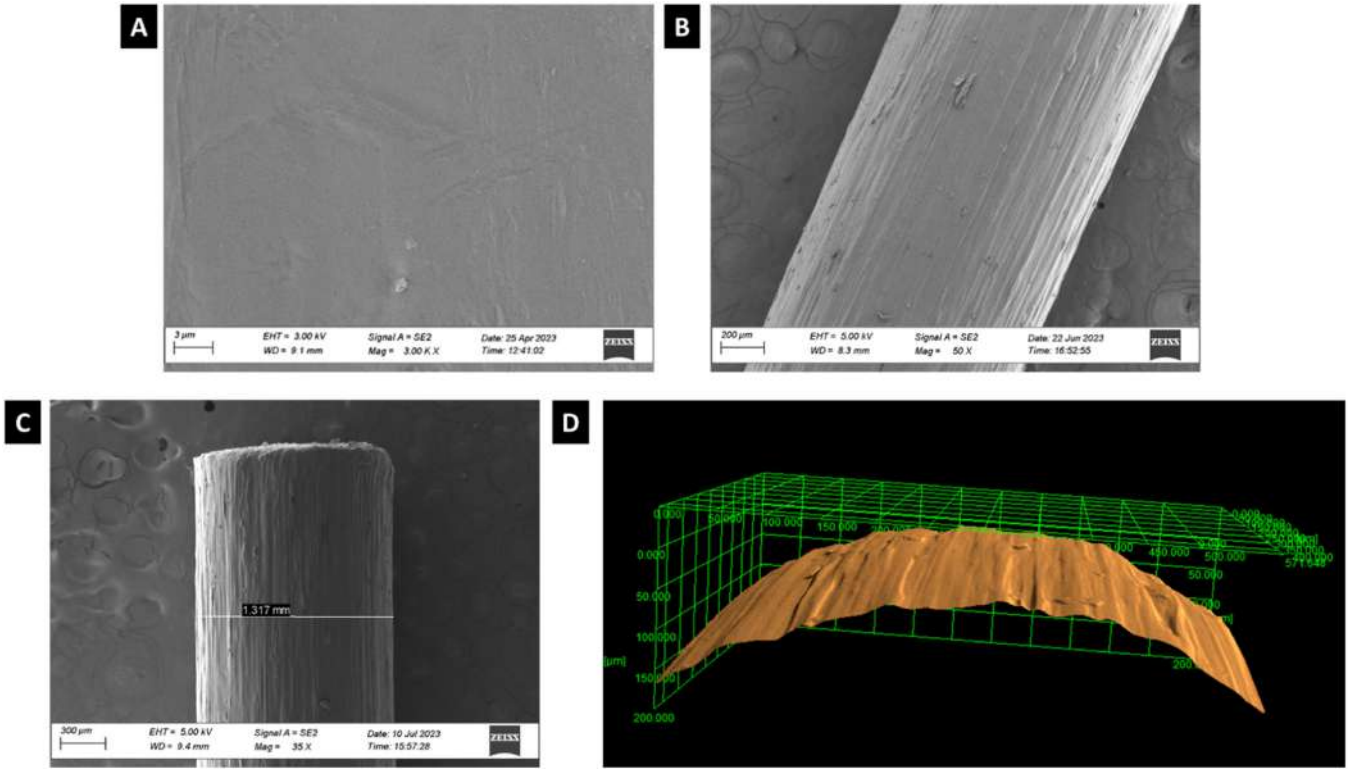

Figure 9. SEM micrographs of the developed inserts (A) and (B) Surface (Scale bar: 3 μm and 200 μm respectively), (C) Edge (Scale bar: 300 μm), (D) 3D SEM image demonstrating the surface topography.

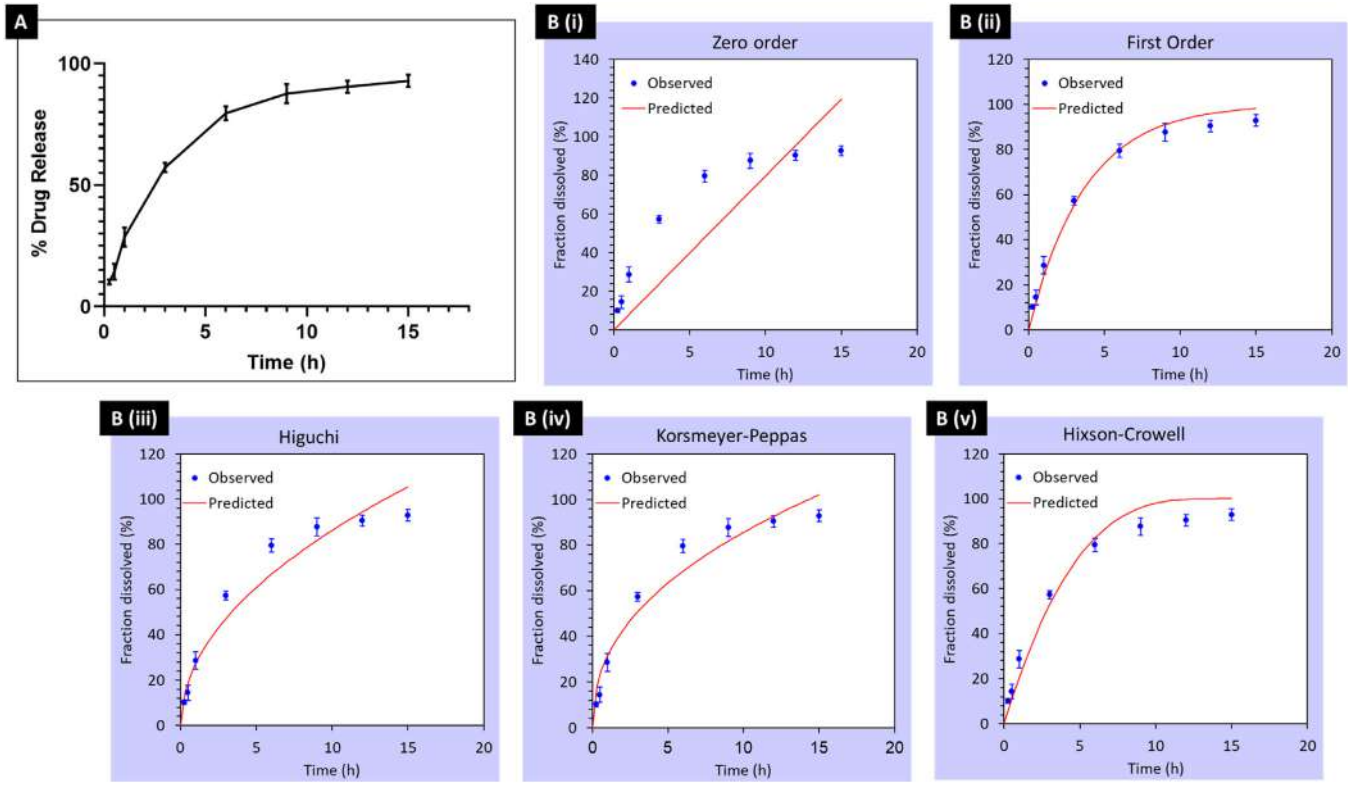

Figure 10. (A) *In vitro* drug release from the developed ocular insert. (B) The drug release values, both the ones that were observed and the ones that were predicted, are presented along with the model prediction using (B, i) Zero order, (B, ii) First order, (B, iii) Higuchi, (B, iv) Korsmeyer-Peppas and (B, v) Hixson-Crowell.

devices.[51] This distinctive characteristic arises from the inherent stability of the surface area of such devices throughout the release process. Conversely, in systems utilizing hydrophilic polymers, such as the HPC insert examined in this investigation, the constantly changing surface area due to swelling introduces a level of complexity that precludes the establishment of a strict Zero-order release pattern and follows a First order mechanism. Further, hydrophilic polymers, when immersed in an aqueous environment, tend to exhibit a pronounced propensity for water absorption. The kinetics of the drug release from such a system is usually affected by the swelling kinetics of the initially dry polymer, offering possibilities of attaining a uniform rate of release.[51] A multitude of factors converge to shape the intricacy of drug-release kinetics in hydrophilic polymer-based delivery systems. These factors encompass the characteristics inherent to the polymer network, the polymeric relaxation, the aqueous solubility of the drug under consideration, the diffusion coefficient of the drug within the swollen polymer matrix, and the relative velocities governing the penetration of water (solvent diffusion) as compared to the diffusion of the drug itself.[52]

Ocular inserts administered in the morning, capable of remaining in the eyes for up to 12–15 h, offer an ideal therapy for DED, providing all-day relief and eliminating the need for frequent eye drop applications. During the eye irritation study in rabbits, it was observed that the instilled insert dissolved within the targeted timeframe of 12–15 h. This dissolution profile can serve as the basis for *In Vitro-In Vivo Correlation* (IVIVC) hypothesis. However, it is essential to conduct *in vivo* studies to validate and confirm the precise correlation.

The release mechanism of the developed inserts was investigated using DDSolver software through regression analysis. Five conventional release models, namely Zero-order, First-order, Higuchi, Hixson-Crowell, and Korsmeyer-Peppas, were applied to fit the release profiles as shown in Table 1. In order to predict the drug release kinetics, the selection of the best model involves considering the highest R^2 value and the smallest AIC (Akaike Information Criterion) value. Additionally, a suitable model is determined when the MSC (modified reciprocal form of AIC) value is greater than 2 or 3. The mathematical model fitting revealed that the release profile from the inserts followed a First-order model. Fig. 10B(i-v) displays multiple graphs, each representing distinct kinetic models.

In vivo *Eye Irritancy Test*

The rabbits' eyes were inspected for any signs of irritation after 72 h of instilling the ocular inserts. Throughout the entire evaluation period, the overall irritation scores for the irritancy test remained at

Table 1
Statistical parameters of models to describe the release of drug from inserts.

Sr. no.	Model	Statistical parameters of models (mean ± SD)		
		R^2	AIC	MSC
1.	Zero Order	0.570 ± 0.026	67.78 ± 0.591	0.595 ± 0.060
2.	First Order	0.983 ± 0.003	41.93 ± 1.027	3.827 ± 0.143
3.	Higuchi	0.940 ± 0.011	52.67 ± 1.528	2.484 ± 0.193
4.	Korsmeyer-Peppas	0.938 ± 0.007	52.22 ± 0.898	2.541 ± 0.107
5.	Hixson-Crowell	0.956 ± 0.008	49.44 ± 1.394	2.888 ± 0.188

0 as evaluated for the cornea, iris, and conjunctiva. Findings revealed no apparent indications of redness or opacity in the cornea. Additionally, the iris and conjunctival blood vessels appeared normal, with no observed swelling in the eyelids. No adverse reactions were documented, and there was no notable distinction between the treated and untreated eyes. Consequently, the findings of the irritancy test demonstrated that the insert was non-toxic and did not cause irritation. However, the irritancy test does not clearly assess the level of comfort/discomfort of the insert. Furthermore, the inserts remained securely in the conjunctival sac of the eye and did not expel out, suggesting that the dimensions of the developed inserts were appropriate.

Conclusion

The study aimed to develop innovative ocular inserts using HME and CaliCut technology, loaded with castor oil and HPC, for managing DED. The preparation of castor oil-loaded ocular inserts was successfully achieved through a continuous HME process in combination with CaliCut. Castor oil was selected for its lubricating and anti-inflammatory properties, while HPC served as the matrix material due to its biocompatibility and potential for managing DED. Optimized parameters during HME ensured smooth extrusion, and CaliCut's precise cutting produced inserts with accurate dimensions. Laser measurement and adjustments in belt speed maintained the desired diameter of the inserts. The inserts demonstrated desirable physicochemical and mechanical behaviour. Irritancy tests on rabbit eyes showed no signs of irritation, confirming the non-toxic and non-irritating nature of the inserts. These inserts offer several advantages, including sustained drug release, improved patient compliance, and reduced inconvenience compared to conventional eye drops. The research is pioneering as it utilizes CaliCut as a post-extrusion system for developing ocular inserts, presenting a promising approach to address the rising incidence of DED. This research might mark a vital stride in the advancement of ocular insert technology, potentially paving the way for more effective treatments for DED.

Declaration of Competing Interest

The authors declare that they have no known competing financial interests or personal relationships that could have appeared to influence the work reported in this paper.

Funding

This research did not receive any specific grant from funding agencies in the public, commercial, or not-for-profit sectors.

Acknowledgement

This work was carried out at the National Institute of Pharmaceutical Education and Research - Ahmedabad (NIPER-A), India. We are grateful to the Department of Pharmaceuticals, Ministry of Chemicals and Fertilizers for funding and support to carry out this research work.

Supplementary Materials

Supplementary material associated with this article can be found in the online version at doi:10.1016/j.xphs.2023.12.015.

References

1. Pult H, Wolffsohn JS. The development and evaluation of the new Ocular Surface Disease Index-6. *Ocul Surf*. 2019;17(4):817–821.
2. Craig JP, Nichols KK, Akpek EK, et al. TFOS DEWS II definition and classification report. *Ocul Surf*. 2017;15(3):276–283.
3. Craig JP, Nelson JD, Azar DT, et al. TFOS DEWS II report executive summary. *Ocul Surf*. 2017;15(4):802–812.
4. Uchino M, Schaumberg DA. Dry eye disease: impact on quality of life and vision. *Curr Ophthalmol Rep*. 2013;1(2):51.
5. Lee BS, Kabat AG, Bacharach J, Karpecki P, Luchs J. Managing dry eye disease and facilitating realistic patient expectations: a review and appraisal of current therapies. *Clin Ophthalmol*. 2020;14:119.
6. Coroi MC, Bungau S, Tit M. Preservatives from the eye drops and the ocular surface. *Rom J Ophthalmol*. 2015;59(1):2.
7. Shadambikar G, Marathe S, Patil A, et al. Novel application of hot melt extrusion technology for preparation and evaluation of valacyclovir hydrochloride ocular inserts. *AAPS PharmSciTech*. 2021;22(1):48.
8. Lacrisert. F.D.A. 2002. Available at: https://www.accessdata.fda.gov/drugsatfda_docs/label/2002/18771s12lbl.pdf. 578. Accessed October 04, 2023.
9. Feng X, Zhang F. Twin-screw extrusion of sustained-release oral dosage forms and medical implants. *Drug Deliv Transl Res*. 2018;8(6):1694–1713.
10. Thermo CaliCut. 2019. Available at: https://assets.thermofisher.com/TFS486Assets/MSD/Technical-Notes/TN623-4005-CaliCut-post-extrusion-system.pdf. Accessed August 11, 2023.
11. Alzahrani A, Youssef AAA, Nyavanandi D, et al. Design and optimization of ciprofloxacin hydrochloride biodegradable 3D printed ocular inserts: full factorial design and in-vitro and ex-vivo evaluations: part II. *Int J Pharm*. 2023;631: 122533.
12. Li D, Guo G, Fan R, et al. PLA/F68/Dexamethasone implants prepared by hot-melt extrusion for controlled release of anti-inflammatory drug to implantable medical devices: I. Preparation, characterization and hydrolytic degradation study. *Int J Pharm*. 2013;441(1–2):365–372.
13. Balasubramaniam J, Srinatha A, Pandit JK, Nath G. In vitro microbiological evaluation of polyvinyl alcohol-based ocular inserts of Ciprofloxacin hydrochloride. *Indian J Pharm Sci*. 2006;68(5):626–630.
14. Taghe S, Mirzaeei S, Alany RG, Nokhodchi A. Polymeric inserts containing Eudragit® L100 nanoparticle for improved ocular delivery of azithromycin. *Biomed*. 2020;8(11):466.
15. Patel UL, Chotai NP, Nagda CD. Design and evaluation of ocular drug delivery system for controlled delivery of gatifloxacin sesquehydrate: in vitro and in vivo evaluation. *Pharm Dev Technol*. 2011;17(1):15–22.
16. Franca JR, Foureaux G, Fuscaldi LL, et al. Bimatoprost-loaded ocular inserts as sustained release drug delivery systems for glaucoma treatment: in vitro and in vivo evaluation. *PLoS One*. 2014;9(4):e95461.
17. Wu X, Zhao G, Wang X, Liu W. Preparation of high-temperature lubricants by blending castor oil with lithium bis(trifluoromethylsulfonyl)imide. *Tribol Lett*. 2017;65(2):1–10.
18. Shah B, Khunt D, Misra M, Padh H. Application of Box-Behnken design for optimization and development of quetiapine fumarate loaded chitosan nanoparticles for brain delivery via intranasal route. *Int J Biol Macromol*. 2016;89:206–218.
19. Thakkar R, Komanduri N, Dudhipala N, Tripathi S, Repka MA, Majumdar S. Development and optimization of hot-melt extruded moxifloxacin hydrochloride inserts, for ocular applications, using the design of experiments. *Int J Pharm*. 2021;603: 120676.
20. Taghe S, Mirzaeei S, Ahmadi A. Preparation and evaluation of nanofibrous and film structured ciprofloxacin hydrochloride inserts for sustained ocular delivery: pharmacokinetic study in Rabbit's Eye. *Life*. 2023;13(4):913.
21. Karnik I, Youssef AAA, Joshi P, et al. Formulation development and characterization of dual drug loaded hot-melt extruded inserts for better ocular therapeutic outcomes: sulfacetamide/prednisolone. *J Drug Deliv Sci Technol*. 2023;84: 104558.
22. Kulhari H, Pooja D, Narayan H, Meena L, Prajapati SK. Design and evaluation of ocusert for controlled delivery of flurbiprofen sodium. *Curr Eye Res*. 2011;36(5):436–441.
23. Gilhotra R, Nagpal K, Mishra D. Azithromycin novel drug delivery system for ocular application. *Int J Pharm Investig*. 2011;1(1):22.
24. Anup N, Gadeval A, Tekade RK. A 3D-printed graphene BioFuse implant for post-surgical adjuvant therapy of cancer: proof of concept in 2D- and 3D-spheroid tumor models. *ACS Appl Bio Mater*. 2022;6:1195–1212.
25. Agarwal R, Rana D, Salave S, Benival D. Dexamethasone loaded electrospun nanocomposite ocular insert: in-vitro drug release and mechanical assessment. *Curr Nanomedicine*. 2022;12(2):150–158.
26. Sangole S, Salave S, Rana D, Shah S, Medhe TP, Benival D. Electrospun nanofiber composite for levofloxacin in ocular drug delivery. *Pharm Nanotechnol*. 2022;10(5):393–400.
27. Jadhav A, Salave S, Rana D, Benival D. Development and in-vitro evaluation of dexamethasone enriched nanoemulsion for ophthalmic indication. *Drug Deliv Lett*. 2023;13:196–212.
28. Rana D, Salave S, Jain S, Shah R, Benival D. Systematic development and optimization of teriparatide-loaded nanoliposomes employing quality by design approach for osteoporosis. *J Pharm Innov*. 2022:1–15.
29. Mundada AS, Shrikhande BK. Design and evaluation of soluble ocular drug insert for controlled release of ciprofloxacin hydrochloride. *Drug Dev Ind Pharm*. 2006;32(4):443–448.
30. Test No. 405: Acute eye irritation/corrosion. 2023. Available at: https://www.oecd.org/env/test-no-405-acute-eye-irritation-corrosion-9789264185333-en.htm. Accessed August 11, 2023.
31. Sandford EC, Muntz A, Craig JP. Therapeutic potential of castor oil in managing blepharitis, meibomian gland dysfunction and dry eye. *Clin Exp Optom*. 2021;104(3):315–322.

32. Goto E, Shimazaki J, Monden Y, et al. Low concentration homogenized castor oil eye drops for noninflamed obstructive meibomian gland dysfunction. *Ophthalmology*. 2002;109(11):2030–2035.
33. Maïssa C, Guillon M, Simmons P, Vehige J. Effect of castor oil emulsion eyedrops on tear film composition and stability. *Cont Lens Anterior Eye*. 2010;33(2):76–82.
34. Loreti G, Maroni A, Del Curto MD, Melocchi A, Gazzaniga A, Zema L. Evaluation of hot-melt extrusion technique in the preparation of HPC matrices for prolonged release. *Eur J Pharm Sci*. 2014;52(1):77–85.
35. Abelson MB, Udell IJ, Weston JH. Normal human tear pH by direct measurement. *Arch Ophthalmol*. 1981;99(2):301.
36. Youssef AAA, Thakkar R, Senapati S, Joshi PH, Dudhipala N, Majumdar S. Design of topical moxifloxacin mucoadhesive nanoemulsion for the management of ocular bacterial infections. *Pharmaceutics*. 2022;14(6):1246.
37. Alzahrani A, Adel Ali Youssef A, Senapati S, et al. Formulation development and in vitro-ex vivo characterization of hot-melt extruded ciprofloxacin hydrochloride inserts for ocular applications: part I. *Int J Pharm*. 2023;630: 122423.
38. Zuliani A, Rapisarda M, Chelazzi D, Baglioni P, Rizzarelli P. Synthesis, characterization, and soil burial degradation of biobased polyurethanes. *Polymers*. 2022;14(22):4948.
39. Jahangirian H, Saleh B, Kalantari K, et al. Enzymatic synthesis of ricinoleyl hydroxamic acid based on commercial castor oil, cytotoxicity properties and application as a new anticancer agent. *Int J Nanomedicine*. 2020;15:2935–2945.
40. Chen YC, Tai W. Castor oil-based polyurethane resin for low-density composites with bamboo charcoal. *Polym*. 2018;10(10):1100.
41. Linn Yusuf AK, Mamza P, Ahmed AS, Agunwa U. Extraction and characterization of castor seed oil from wild Ricinus Communis. *Int J Sci Environ*. 2015;4:1392–1404.
42. Eguchi N, Kawabata K, Goto H, Eguchi N, Kawabata K, Goto H. Electrochemical polymerization of 4,4-dimethyl-2,2'-bithiophene in concentrated polymer liquid crystal solution. *J Mater Sci Chem Eng*. 2017;5(2):64–70.
43. Alharbi ND, Guirguis OW. Macrostructure and optical studies of hydroxypropyl cellulose in pure and nano-composites forms. *Results Phys*. 2019;15: 102637.
44. Dawud H, Abu Ammar A. Rapidly dissolving microneedles for the delivery of steroid-loaded nanoparticles intended for the treatment of inflammatory skin diseases. *Pharmaceutics*. 2023;15(2):526.
45. Goyanes A, Allahham N, Trenfield SJ, Stoyanov E, Gaisford S, Basit AW. Direct powder extrusion 3D printing: fabrication of drug products using a novel single-step process. *Int J Pharm*. 2019;567: 118471.
46. Aburahma MH, Mahmoud AA. Biodegradable ocular inserts for sustained delivery of brimonidine tartarate: preparation and in vitro/in vivo evaluation. *AAPS PharmSciTech*. 2011;12(4):1335.
47. Jethava JK, Jethava GK. Design, formulation, and evaluation of novel sustain release bioadhesive in-situ gelling ocular inserts of ketorolac tromethamine. *Int J Pharm Investig*. 2014;4(4):226.
48. Makadia HK, Siegel SJ. Poly Lactic-co-Glycolic Acid (PLGA) as biodegradable controlled drug delivery carrier. *Polymers*. 2011;3(3):1377.
49. Veiseh O, Vegas AJ. Domesticating the foreign body response: recent advances and applications. *Adv Drug Deliv Rev*. 2019;144:148–161.
50. Carnicer-Lombarte A, ST Chen, Malliaras GG, Barone DG. Foreign body reaction to implanted biomaterials and its impact in nerve neuroprosthetics. *Front Bioeng Biotechnol*. 2021;9: 622524.
51. Sanopoulou M, Papadokostaki KG. Controlled drug release systems: mechanisms and kinetics. ed. In: Stamatialis D, ed. *Biomed. Membr. (Bio)artificial Organs*. Singapore: World Scientific; 2017:1–33.
52. Mathematical models of drug release. ed. In: Bruschi ML, ed. *Strategies to Modify the Drug Release from Pharmaceutical Systems*. Cambridge: Woodhead Publishing; 2015:63–86.

Journal of Pharmaceutical Innovation
https://doi.org/10.1007/s12247-022-09663-9

ORIGINAL ARTICLE

Systematic Development and Optimization of Teriparatide-Loaded Nanoliposomes Employing Quality by Design Approach for Osteoporosis

Dhwani Rana[1] · Sagar Salave[1] · Sonali Jain[2] · Ravi Shah[2] · Derajram Benival[1,3]

Accepted: 10 June 2022

Abstract

Purpose The present study is aimed at developing liposomal nanovesicular system of teriparatide employing the use of ethanol injection method for providing sustained release in the treatment of osteoporosis.

Methods Formulation development was carried out systematically by employing Quality by Design (QbD) approach. The developed system was evaluated for various physicochemical characterizations.

Results The developed liposomal formulation exhibited particle size of approximately 186.9 ± 2.20 nm. Cryogenic field emission scanning electron microscopy (Cryo-FE-SEM) analysis revealed spherical morphology of the liposomes. The % encapsulation efficiency (% EE) was found to be 46.52% and polydispersity index (PDI) to be 0.149 ± 0.02, suggesting narrow particle size distribution of the developed liposomal formulation. Circular dichroism study revealed intact structure of drug in the formulation. Haemolysis assay was performed and the no significant lysis of RBC was observed up to the concentration of 10 µg/ml of formulation. The developed formulation took almost 24 h to release 50% of the encapsulated teriparatide while it took 36 h to release about 90% of the drug. Furthermore, results of cell viability study suggest that encapsulation of teriparatide into the liposomes is not affecting its safety.

Conclusion The implementation of the QbD concept in the development of teriparatide-loaded liposomes enhanced understanding of the manufacturing process and the influence of formulation parameters on the quality attributes of liposomes.

Keywords Osteoporosis · Teriparatide · QbD · Sustained release · Liposomes

Introduction

The basis for healthy bones lies in maintaining optimal levels of bone mass. Bone is a dynamic tissue undergoing constant change and continuous structural remodeling [1]. In most individuals, over the age of 30, peak bone mass is usually attained. However, bone remodeling persists after that, and loss of bone mass is slightly more than the gain. Osteoporosis is a complex, bone-incapacitating disease that silently progresses and shows no clinical symptoms until the incidence of fracture occurs. This multifactorial systemic skeletal disease results from a disturbance in the bone remodeling cycle, causing microarchitectural deterioration of bone tissue. The characteristic of osteoporosis is reduced bone mineral density (BMD) leading to poor bone strength, increased bone fragility, and susceptibility to fracture. The poor bone strength manifests towards increased proneness of fractures of the spine, hip, forearm, and other skeletal settings ultimately leading to morbidity and mortality [2]. Bone tissue undergoes dynamic regulation by the bone formation and bone resorption, and osteoporosis transpires when the resorption rate surpasses the formation rate [3, 4]. This compromised remodeling aiding bone resorption more than bone formation is the ultimate pathophysiological mechanism causing osteoporosis [5]. Various therapeutic interventions are available which attempts to regulate the bone

✉ Derajram Benival
derajram@niperahm.res.in

[1] Department of Pharmaceutics, National Institute of Pharmaceutical Education and Research (NIPER), Ahmedabad, India

[2] Department of Pharmaceutical Analysis, National Institute of Pharmaceutical Education and Research (NIPER), Ahmedabad, India

[3] Department of Pharmaceuticals, Ministry of Chemicals and Fertilizers, Opp. Airforce Station, Palaj, Gandhinagar - 382355, Gujarat, India

remodeling process. This can be achieved either by inhibiting the bone resorption or by stimulating bone formation, establishing benefits in treating osteoporosis. The suppression of osteoclast-mediated bone resorption and reduction in bone turnover can be achieved by antiresorptive agents. This therapeutic class includes bisphosphonates, RANK ligand inhibitors, estrogens, selective estrogen receptor modulators, monoclonal antibodies, and calcitonin [6, 7]. For effective treatment of osteoporosis, there must be an equilibrium among bone resorption and bone formation. Hence, along with resorption inhibitors, stimulators of bone formation are significantly impactful to the patients who have lost a substantial amount of bone. As the anabolic agents maintain a positive balance of bone remodeling, they are considered more effective [8]. Anabolic agents are capable of restoring BMD, bringing it back to a normal level. Furthermore, they reduce the frequency of osteoporotic fracture more than that of the currently available antiresorptive agents [9, 10].

Among all anabolic agents, teriparatide is the most extensively utilized. It is an analog of endogenous parathyroid hormone (PTH) made up of the first 34 amino acids of the 84 amino acid human PTH [11]. Teriparatide being a peptide rapidly gets digested by proteolytic enzymes present in the gastrointestinal tract, and therefore, currently, it is administered daily as a subcutaneous injection for the maximum duration of 2 years [12]. This method of delivery compromises patient compliance. To promote patient adherence, a once-weekly teriparatide (TERIBONE) formulation was introduced in Japan. Instead of 20 μg daily, this once-weekly treatment uses 56.5 μg [13]. But the larger amount caused nausea and vomiting, forcing patients to stop treatment. In 2019, a twice-weekly formulation (TERIBONE autoinjector) was released to combat these side effects [14, 15]. Because these are all aqueous solutions, teriparatide is absorbed and eliminated from the body within 3 h, giving it an extremely short half-life.

Kostenuik et al. hypothesized that anabolic effects similar to the daily injection of teriparatide could be achieved with a long-acting formulation with less frequency of administration [16]. The authors covalently linked teriparatide with the Fc segment of human IgG1 and subcutaneous injection of this conjugate increased half-life. While the scientists showed that covalently conjugated teriparatide was as effective as unmodified teriparatide in activating PTH receptors in vitro, such modification in a molecule makes it a completely new drug and warrants completely new safety evaluation studies. However, drug delivery technologies like liposomes, nanoparticles, and microspheres do not require covalent alteration of molecules to increase pharmacokinetic properties and so require minimal safety assessments [17, 18]. The provision to load hydrophilic and hydrophobic drugs, as well as the utilization of biocompatible and biodegradable phospholipids as building blocks, makes liposomes a popular drug delivery technology [19]. Liposomes are an excellent choice for providing sustained release drug delivery. Barbălată et al. developed liposomes loaded with (-)-epigallocatechin gallate (EGCG) as a functional ingredient by using the Quality by Design (QbD) approach. The release profile illustrated a continuous and sustained release of EGCG from the optimal formulation for at least 72 h [20]. Tamoxifen citrate-loaded sustained release liposomes have been developed and tested for their physicochemical properties. The developed formulation demonstrated 50% drug release within 3 h and 95% drug release within 30 h, indicating the usefulness of the developed system for sustaining the in vitro release of tamoxifen citrate [21]. Karumanchi et al. encapsulated the protein drug bevacizumab within the liposomes to obtain drug release over a prolonged period for treating ocular angiogenesis [22]. Sun et al. developed a bone-targeting drug delivery system using biomineral-binding liposomes loaded with icariin to improve osteoporosis treatment. Icariin, a flavonoid glycoside that has been shown to promote osteoblast maturation, was encapsulated in the liposomal formulation. The in vitro release investigation found that icariin from liposomes had an excellent sustained release profile for up to 96 h [23]. Multivesicular liposomes for sustained drug delivery of cytarabine hydrochloride were fabricated by Assil et al. Results demonstrated that almost 30% of the cytarabine remained in the conjunctiva and episcleral tissues after 72 h. This controlled rate of drug release may reduce ocular toxicity while increasing the drug's efficacy in ocular proliferative disorders [24]. Moreover, DepoDur extended-release liposome injection is a sterile suspension of multivesicular liposomes using proprietary DepoFoam® formulation technology containing morphine sulfate. The formulation intended for epidural administration provides effective postoperative analgesia for 48 h [25, 26]. Liposome-based vesicular delivery has not been reported previously for extending the release of teriparatide. Thus, this work deals with the development of a nano-liposomal formulation of teriparatide for sustained release using the ethanol injection technique by employing the systematic approach of QbD.

Materials and Methods

Materials

Teriparatide (molecular weight 4117.8 Da) was obtained from Sigma Aldrich (St. Louis, MO, USA). Soybean phosphatidylcholine (SPC) was obtained from Lipoid S100, cholesterol from Sigma-Aldrich (St. Louis, MO, USA), ethanol from Loba Chemie (Mumbai, India), and chloroform from Emparta (Darmstadt, Germany). Sodium chloride (NaCl) was obtained from HiMedia Laboratories Pvt.

Ltd. (Maharashtra, India), and potassium chloride (KCl), sodium hydrogen phosphate (Na_2HPO_4), potassium dihydrogen phosphate (KH_2PO_4), glacial acetic acid, methanol, acetonitrile, formic acid, as well as isopropyl alcohol were procured from Fischer Scientific (Loughborough, Leicestershire). Dulbecco's modified Eagle's medium (DMEM), trypsin, and fetal bovine serum (FBS) were purchased from Invitrogen, Thermo-Fischer Scientific (Waltham, MA, USA). All the reagents and solvents used in this work were of analytical grade. Throughout the study, Milli Q (ultrapure water) was used which was obtained from Merck Millipore System (Darmstadt, Germany).

Methods

Development of Liposomes Using QbD steps

The development of liposomes was done using QbD approach following Guidance for Industry-Liposomal Drug Products by Food and Drug Administration (FDA) and International Council for Harmonisation (ICH) guidance for industry, Q8(R2) Pharmaceutical Development [27, 28]. The QbD-based development included defining of quality target product profile (QTPP), identifying potential critical quality attributes (CQAs), performing risk assessment for identifying formulation variables, material attributes, and process parameters affecting CQAs of the drug product, establishing critical material attributes (CMAs) and critical process parameters (CPPs), establishing design space having product specifications and setting control strategy for ensuring continuous improvement. For understanding the relationship between CMAs and CPPs and studying their impact on CQAs mathematically, design of experiment (DoE) strategy was employed [20, 29]. As per the existing flux of scientific literature for the development of liposomes, QTPP is set as described in Table 1.

For preparing liposomes, various methods like thin-film hydration, ethanol injection, and freeze–thaw method were explored, and based on feasibility, considering physicochemical stability of teriparatide, desired particle size for the subcutaneous route, and %EE of the drug into liposomes, ethanol injection method was chosen [30]. First of all, an aqueous phase was prepared. For this, a solution of sodium acetate anhydrous (1 M, 4.1017 gm in 50 ml Milli-Q water) was mixed with glacial acetic acid (1 M, 0.5714 ml in 10 ml Milli-Q water) to obtain acetate buffer pH 4.0. The required amount of teriparatide was weighed and added into the buffer solution to obtain a clear aqueous phase.

For the organic phase, desired amount of SPC and cholesterol was weighed and added into 1 ml of absolute ethanol. The obtained mixture was then vortexed until a clear solution was obtained. The resulting clear organic phase was injected by the means of a syringe needle into the aqueous phase which was subjected to continuous stirring at different rpm for 15 min maintained at 2–8 °C temperature. This addition of the organic phase into the aqueous phase resulted in the spontaneous formation of liposomes [31]. The obtained colloidal liposomal dispersion was centrifuged and obtained supernatant was injected in high performance liquid chromatography (HPLC) for the determination of % EE.

Preliminary Screening of Parameters

The factors influencing the formation of liposomes were studied. This includes process-related parameters such as stirring speed, stirring time, temperature, rate of injection of organic phase into aqueous phase, and formulation-related factors such as concentration of the drug, concentration of lipid, concentration of cholesterol, amount of aqueous phase, amount of organic phase, and the ratio of aqueous to organic phase volume. The influence of process parameters as well as formulation variables on properties of formed liposomes was assessed for particle size, %EE, zeta potential, and PDI. One-factor-at-a-time strategy was applied and the CPP and CMA affecting the formulation outcomes were determined.

Table 1 QTPP of aimed liposomal formulation

QTPP elements	Target	Inference
Formulation	Injectable liposomes	Must meet the set standards from specifications of similar studies and scientific research
Route of administration	Subcutaneous	
Specific properties	Prolonged drug release	
Quality attributes of formulation	**Target**	
%EE (entrapment efficiency)	> 30%	
Vesicular size	< 300 nm	
PDI (poly dispersity index)	< 0.2	
Drug release	> 24 h	
Haemocompatibility	Lack of haemolytic activity	

Experimental Design

Formulation optimization was carried out using three level Box–Behnken design (BBD) to investigate the response surfaces by employing Design Expert software (Version 12, Stat-Ease, Inc., Minneapolis, MN, USA). [32]. The independent variables viz (A) drug concentration, (B) lipid concentration, (C) cholesterol concentration, and (D) stirring speed of magnetic stirrer were screened and selected based on the preliminary studies. Other factors such as stirring time, phase volume ratio, and rate of injection of organic phase were kept constant. The impact of each of these four quantitative independent factors on CQAs such as R1: particle size and R2: %EE was investigated. Every variable was examined at two levels, low (− 1) and high (+ 1). Following BBD, 27 experimental runs including three replicates were performed and the result of individual input factors on CQAs was evaluated independently and in confounding. For this, analysis of variance (ANOVA) was explored and the level of significance of the model for every factor was also determined.

Three-dimensional response surface plots were obtained depicting the interaction influence of independent variables on respective responses. The preferred range of CQAs were set and design space (overlay plot) was created to assess the quality of the product and to obtain the optimized formula.

Optimization of Design and Model Validation

For ensuring the quality of generated design space, validation of model and design space was performed. The precision of the model was evaluated by performing confirmatory experiments and comparing the results acquired from optimized formulation to that of predicted responses.

Physicochemical Characterization of Optimized Formulation

Particle Size and Size Distribution

The particle size and PDI of prepared liposomes were observed by dynamic light scattering (DLS) method employing Malvern Zetasizer Nano ZS 90 (Malvern Instrument). The prepared liposomes were subjected to dilution using Milli-Q water prior to size measurement to produce an appropriate scattering intensity. Measurements were taken using 1 ml of diluted liposomal preparation into disposable polystyrene cuvette. Each sample was measured in triplicate at 25 °C with a scattering angle of 90°. The PDI and mean hydrodynamic diameter (Z-average) were measured.

Cryogenic Field Emission Scanning Electron Microscopy (Cryo FE-SEM)

The morphological characteristics of prepared liposomes were inspected by scanning electron microscopy (SIGMA S300, Zeiss). The sample was frozen before imaging. Sample preparation included transferring of sample into rivets mounted on cryo SEM sample holder. The sample was further submerged into a slush vent containing liquid nitrogen for freezing. The frozen sample was fractured at − 150 °C with the help of a cold knife, followed by sublimation for 10 min at − 90 °C in order to etch away water. The temperature was allowed to come to a steady state by lowering it to − 130 °C. Afterward, the sample was sputter-coated to deposit a thin layer of platinum at 10 mA for 90 s [33]. Images were obtained after subjecting the sample to a high vacuum cryo FE-SEM microscopic chamber.

%EE Determination

To calculate the %EE of various batches of liposomal formulation, unentrapped/free drug in the supernatant was determined. To obtain supernatant, the colloidal liposomal dispersion was subjected to centrifugation at 14,000 rpm for 30 min at 4 °C. The resultant supernatant was carefully collected and drug concentration in the supernatant was determined by HPLC in a gradient mode (HPLC 1260 Infinity, Agilent Technologies). For the HPLC analysis, a reverse phase XBridge BEH C18 column (300 Å, 4.6 mm × 150 mm, 10 µm,) was used. The composition of the mobile phase was 0.1% v/v formic acid in Milli Q water as aqueous phase (A) and 0.1% v/v formic acid in acetonitrile as organic phase (B). An injection volume of 10 µl and diode array detector which was tuned to 210 nm was used. The run time was set for 15 min in gradient mode. Openlab software was used for data acquisition and data processing. %EE was calculated using the equation mentioned below:

$$\%EE = \frac{\text{Amount of total drug} - \text{Amount of unentrapped drug}}{\text{Amount of total drug added}} X100$$

Circular Dichroism Spectroscopy

Circular Dichroism Spectrometer-J 815 (Jasco) equipped with a 150 W Xenon lamp was employed to examine the stability of teriparatide. Pure teriparatide was used as a standard. The drug extracted from the liposomes was used as sample and was evaluated at wavelength 190–250 nm.

Haemolysis Assay

Haemolysis assay of the optimized formulation was performed as a part of blood compatibility studies. Fresh blood from Sprague–Dawley rats was collected in EDTA tube and was subjected to centrifugation at 2500 rpm in order to separate plasma. The obtained RBC suspension was diluted with phosphate buffer saline (PBS). A total of 0.4 ml of RBC suspension was added to 1.6 ml samples of various concentrations. A total of 1.6 ml of deionized water with 0.4 ml RBC suspension and 1.6 ml PBS with 0.4 ml RBC suspension were used as positive and negative controls respectively. Every concentration was assessed in triplicate. All the samples were incubated for 2 h at 37 °C. After the incubation period, the tubes were centrifuged at 2500 rpm for 5 min and the absorbance of the supernatant was recorded at 541 nm using a multimode UV microplate reader (Varioskan LUX, Thermo Fischer Scientific). The percentage of haemolysis was measured by the following equation [34, 35] :

$$\% \text{ Haemolysis} = \frac{\text{Absorbance of sample} - \text{Absorbance of negative control}}{\text{AAbsorbance of positive control} - \text{Absorbance of negative control}} \text{ X } 100$$

In Vitro Drug Release Study

The obtained liposomal dispersion was centrifuged at 14,000 rpm for 30 min at 4 °C. The settled liposomal pellet was re-dispersed in phosphate buffer saline (PBS) pH 7.4 and incubated at 37 °C with shaking at 50 rpm. At predetermined time intervals of 0.25, 0.5, 1, 3, 6, 12, 18, 24, 30, and 36 h, the samples were subjected to centrifugation for collection of supernatants, and the obtained supernatant was substituted by fresh PBS. The supernatant samples were introduced to the HPLC system with the above-mentioned gradient program and method specifications [36]. The released amount of teriparatide from the liposomes was plotted as a function of time and the results are expressed as mean ± SD of triplicate analysis.

The obtained drug release data were analysed by means of DDSolver software to understand the drug release kinetics. Zero order, first order, Korsmeyer-Peppas, and Higuchi and Hixson-Crowell models were used to analyze the release data of the developed liposomal formulation. The obtained results were evaluated for statistical parameters like adjusted coefficient of determination ($R^2_{adjusted}$), Akaike information criterion (AIC), and model selection criteria (MSC) [37].

In Vitro Cell Line Study

To evaluate the impact of developed formulation on fibroblasts, in vitro cell line study was carried out. NIH 3T3 cell line was used to evaluate the cell viability after subjecting the cells to different dilutions of varying concentrations of formulations by the means of alamarBlue assay. DMEM along with 10% FBS and penicillin G/streptomycin was used for growing the NIH 3T3 cell line. The flasks were kept in an incubator at 37 °C ± 2 °C and 5% CO_2 until confluency of > 90% was achieved [38].

AlamarBlue Cell Viability Assay

This quantitative colorimetric assay is based on the biochemical reduction of alamarBlue dye from non-fluorescent blue to fluorescent red by metabolically active cells. The NIH 3T3 cells were seeded in a 96-well plate (Falcon®), each well receiving 10^4 cells and incubated for 24 h. The cells were treated with plain teriparatide at different concentrations of 0.5, 5, and 50 µg/ml and liposomal formulation at concentrations of 0.5, 5, and 50 µg/ml and kept in an incubator for 24 h. The wells containing media (without formulation) were considered as control. Media was removed and cells were given a wash with PBS. Then, all wells were treated with alamarBlue reagent and kept in an incubator for 4 h. The fluorescence intensity of the solutions in every well was determined using a multimode UV microplate reader (Varioskan LUX, Thermo Fischer Scientific) at 520–590 nm. The cell viability was obtained from the following equation:

$$\% \text{ Viability} = \frac{\text{Average of samples treated with formulation}}{\text{Average of control}} \text{ X } 100$$

Results and Discussion

QbD Steps for Liposomal Development

In the formulation development process, all the material attributes and process parameters which could influence the CQAs of the aimed product were studied for the generation of knowledge space. A cause and effect Ishikawa diagram (Fig. 1) was constructed for risk assessment [20, 39]. Following this, based on risk estimation, CMAs (drug concentration, lipid concentration, and cholesterol concentration) and CPPs (Stirring speed) were chosen by qualitatively evaluating their impact on the CQAs identified by the Ishikawa diagram.

Design of Experiments, Optimization Studies, and Statistical Analysis of Data

In current learning, Box–Behnken's experimental design was conducted for optimization of liposomal formulation and to examine the impacts of dependent variables with regard to

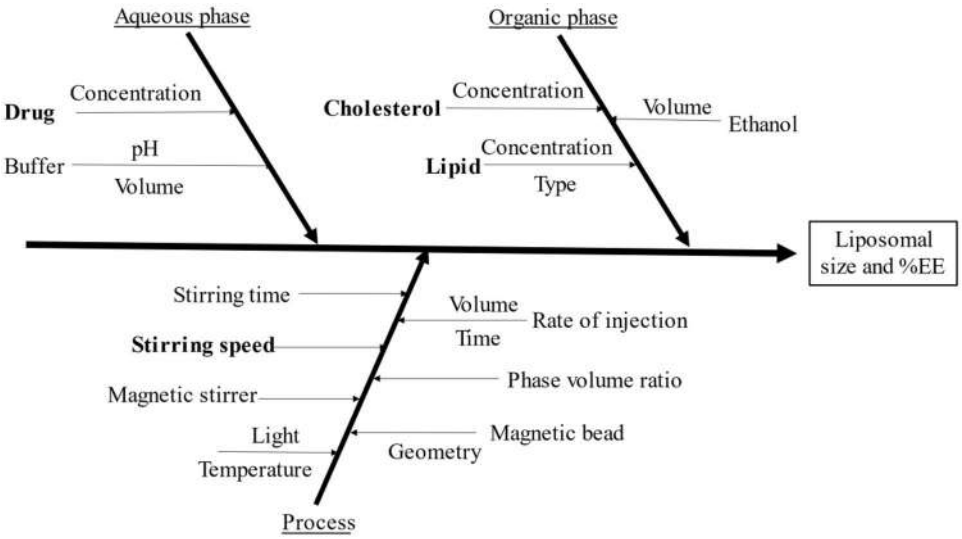

Fig. 1 Ishikawa diagram depicting all the factors influencing CQAs

particle size and %EE. A total of 27 runs were suggested by the DoE and Table 2 shows performed experiments with obtained responses.

It was observed from the obtained responses that CQAs were significantly dependent on the selected factors. However, PDI was found to be ˂ 0.2 in all the cases and no rational

Table 2 BBD matrix for optimization

Run	Factor 1 A: Drug conc µM	Factor 2 B: Lipid conc mM	Factor 3 C: Cholesterol conc mM	Factor 4 D: Stirring speed rpm	Response 1 Particle size nm	Response 2 EE %
1	30	30	15	600	186.9	46.52
2	30	30	20	350	217.1	45.00
3	45	30	10	600	178.8	41.71
4	45	30	10	100	177.6	41.60
5	45	20	15	100	244.4	25.06
6	45	40	20	350	211.0	26.74
7	45	30	15	350	182.1	42.86
8	60	20	15	350	233.4	24.68
9	30	30	10	350	181.6	43.69
10	60	30	10	350	182.1	36.77
11	45	40	10	350	190.3	26.55
12	45	40	15	600	180.2	28.88
13	30	30	15	100	203.2	43.76
14	30	20	15	350	230.9	22.93
15	45	20	15	600	195.8	29.63
16	60	40	15	350	196.9	24.84
17	60	30	20	350	212.4	31.06
18	45	20	20	350	284.0	31.35
19	60	30	15	600	180.7	23.07
20	30	40	15	350	189.5	30.50
21	45	30	15	350	189.8	23.43
22	45	30	15	350	181.1	20.94
23	45	40	15	100	215.9	34.74
24	45	30	20	100	238.1	14.53
25	45	20	10	350	222.3	21.94
26	60	30	15	100	203.3	27.32
27	45	30	20	600	227.3	22.29

Table 3 Dependent variables used in the BBD

Dependent variables				
Responses	**Name**	**Units**	**Minimum**	**Maximum**
R1	Particle size	nm	177.6	284.0
R2	EE	%	15.61	47.01

association could be acquired between an independent variable and the zeta potential. Thus, PDI and zeta potential readings were excluded from the final design. Table 3 depicts the variation range observed in the value of responses.

Furthermore, statistical analysis and evaluation of design were performed using ANOVA and the assumed regression models were found to be statistically significant (p-values < 0.05) for both the responses. Tables 4 and 5 summarizes p-value and F-value for particle size and %EE respectively.

For particle size, reduced quadratic regression model and for %EE, reduced cubic regression model was found appropriate fulfilling all the fitting criteria. The values of R^2, adjusted R^2, and predicted R^2 are shown in Table 8, with a difference lower than 0.2 between adjusted R^2 and predicted R^2. Table 6 summarizes all the important model parameters along with their values for both the CQAs.

Table 6 Statistical data values for CQAs

Parameters	Values for CQAs	
	Particle size	**Entrapment efficiency**
Model *F*-value	27.54	11.05
Model *p*-value	< 0.0001	0.0001
Lack of fit *p*-value	0.1963	0.9903
R^2-unadjusted value	0.8920	0.5904
R^2-adjusted value	0.8596	0.5369
R^2-predicted value	0.7634	0.4653
Adequate precision	21.4056	10.1906

Following ANOVA, polynomial equations having coded factors were generated for both the predetermined responses.

$$\text{Particle size} = 188.76 - 18.92B + 21.43C - 11.07D - 10.25BC + 22.85B^2 + 13.85C^2$$

$$\%EE = 33.63 - 6.08B^2 - 8.83AD^2 - 10.99CD^2$$

Positive sign in the above equations represents synergistic effect whereas negative coefficients represent antagonistic effect. Based on the response surface methodology (RSM)

Table 4 ANOVA for reduced quadratic model: particle size

Source	Sum of squares	df	Mean square	*F*-value	*p*-value	
Model	15,610.72	6	2601.79	27.54	**< 0.0001**	**Significant**
B-Lipid conc	4294.08	1	4294.08	45.45	< 0.0001	
C-Cholesterol conc	5512.65	1	5512.65	58.34	< 0.0001	
D-Stirring speed	1469.65	1	1469.65	15.55	0.0008	
BC	420.25	1	420.25	4.45	0.0478	
B^2	3340.37	1	3340.37	35.35	< 0.0001	
C^2	1226.93	1	1226.93	12.98	0.0018	
Residual	1889.77	20	94.49			
Lack of fit	1844.44	18	102.47	4.52	**0.1963**	**Not significant**
Pure error	45.33	2	22.66			
Cor total	17,500.48	26				

Table 5 ANOVA for reduced cubic model: %EE

Source	Sum of squares	df	Mean square	*F*-value	*p*-value	
Model	1041.33	3	347.11	11.05	**0.0001**	**Significant**
B^2	246.48	1	246.48	7.85	0.0101	
AD^2	311.53	1	311.53	9.92	0.0045	
CD^2	483.31	1	483.31	15.39	0.0007	
Residual	722.53	23	31.41			
Lack of fit	464.83	21	22.13	0.1718	**0.9903**	**Not significant**
Pure error	257.71	2	128.85			
Cor total	1763.86	26				

tool, the influence of all input factors on dependent variables (CQAs) was estimated.

Effect of Formulation and Process Attributes on Particle Size

The analysis of 3-D response surface plots revealed that cholesterol concentration exhibited a high influence on particle size with a rise in cholesterol concentration, resulting in an increase in particle size as depicted in Fig. 2A. Cholesterol interacts with lipid components and modulates membrane fluidity. It gets distributed in the packing of phospholipid bilayer and increases the distance between phospholipid chains, restraining the possibility of interaction among polar head-groups of phosphatidylcholines in the lipid bilayer. As the number of molecules of cholesterol increases, it gets arranged in the phospholipid bilayer, causing an increase in the size of liposomes [31]. It is observed in Fig. 2B that increase in lipid concentration exhibited a slight decrease in particle size up to a certain concentration and further elevation of lipid concentration was found to increase the particle size of liposomes. The results (Fig. 2C) showed that the concentration of drug had no significant impact on particle size of produced vesicles. The stirring speed was found to cause decrease in particle size as depicted in Fig. 2D and this can be attributed to the rapid self-arrangement of lipids on increased stirring rate. Also, high mixing energy and shearing stress might result in the formation of smaller lipid droplets from ethanolic lipid dispersion.

Effect of Formulation and Process Attributes on %EE

The impact of cholesterol concentration on %EE of developed liposomes was ascertained to be negligible (Fig. 3A). With respect to lipid concentration, it was found that increasing lipid concentration to a certain level increased %EE and on subsequent rise in lipid level caused reduction in entrapment of drug in the vesicles (Fig. 3B). From Fig. 3C, it can be noticed that drug concentration had shown insignificant effects on the %EE of liposomes. Stirring speed affected %EE in a way that an increase in stirring speed caused a significant rise in %EE up to the central point and then a downward drift was apparent with further increase in speed of magnetic stirrer (Fig. 3D).

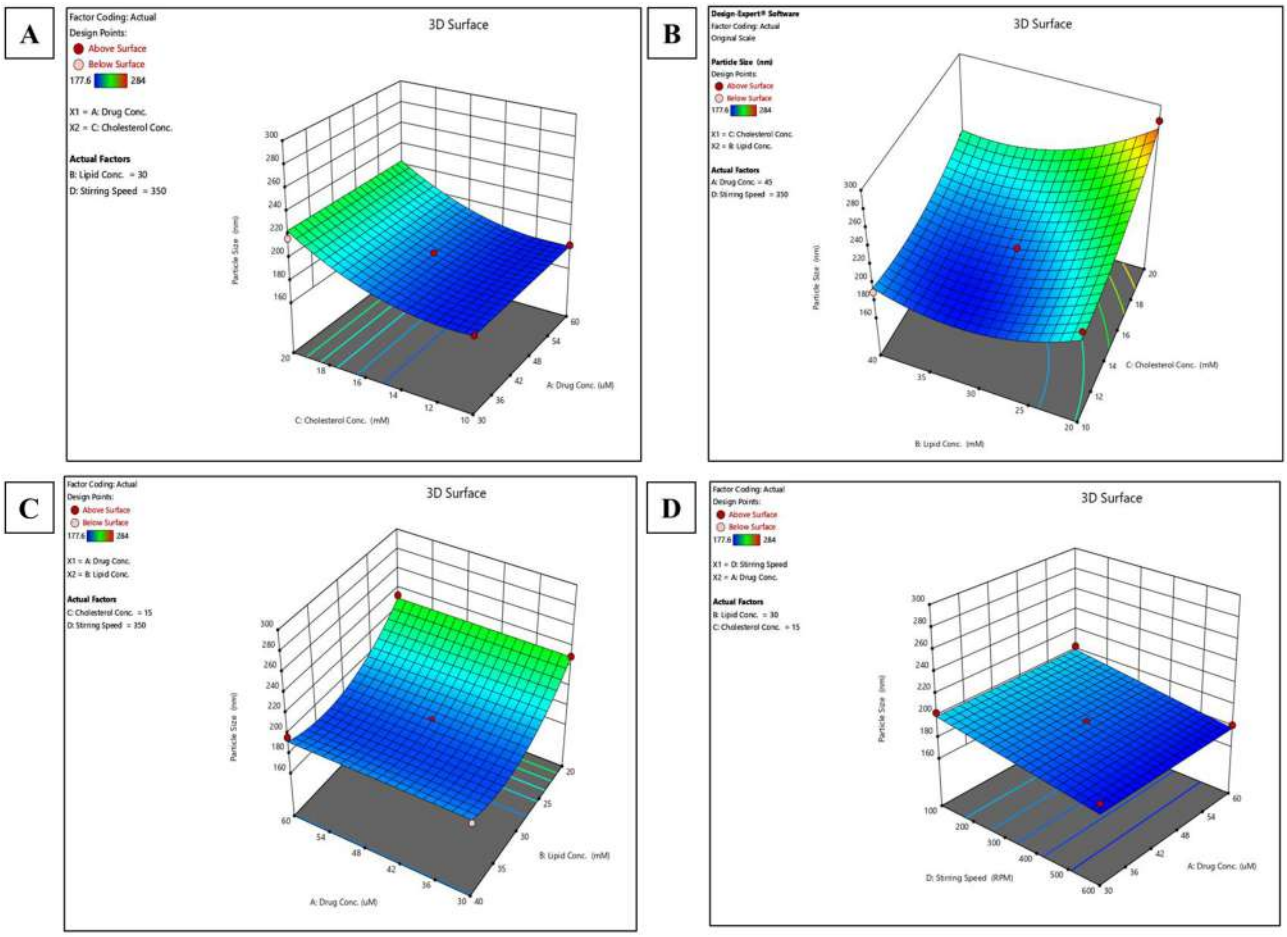

Fig. 2 Effect of **A** cholesterol concentration, **B** lipid concentration, **C** drug concentration, and **D** stirring speed on particle size

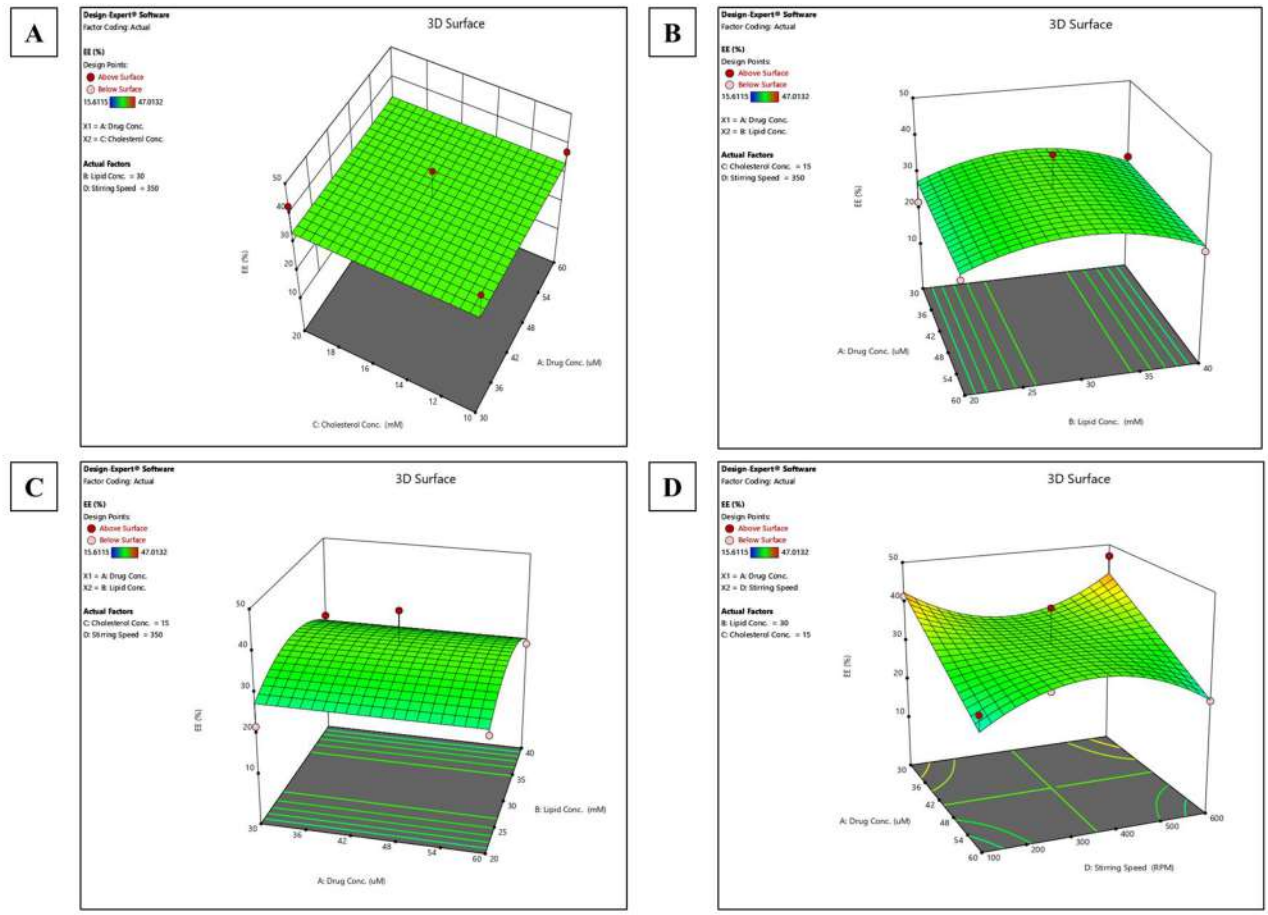

Fig. 3 Effect of **A** cholesterol concentration, **B** lipid concentration on particle size, **C** drug concentration, and **D** stirring speed on %EE

Design Optimization and Model Validation

Optimization of the design was accomplished by generating a design space (overlay plot) as shown in Fig. 4. Design space provides a pluridimensional combination and interaction of predetermined input factors (CPP and CMA) which have been established for assuring product quality [40].

Validation of the model was done by performing confirmatory experiments as summarized in Table 7. Since all the practically attained values were in agreement with anticipated values, the predictability of the model was reinforced, and the model was validated.

Characterization of Liposomes

Cryogenic Field Emission Scanning Electron Microscopy (Cryo FE-SEM)

The developed formulation was characterized by cryo FE-SEM to confirm the formation of vesicles. This visual technique was employed for obtaining details related to surface morphology and the mean size of liposomes. The images (Fig. 5) revealed spherical shape of liposomes having smooth surface and mean diameter in the range of 200–230 nm.

Circular Dichroism Spectroscopy

The structural stability of drug was confirmed by Far-UV circular dichroism spectroscopy. Spectra of pure drug and drug extracted from formulation (Fig. 6) were obtained and both were found to have similar pattern, reflecting no alteration in the secondary structure. It could be inferred that the secondary structure of treated teriparatide persisted to be the same [41].

Haemolysis Assay

Haemolysis increased as the concentration increased from 0.1 to 10 µg/ml; however, the obtained results of % haemolysis was in the satisfactory range, i.e., below 5% for each concentration (Fig. 7c). Figure 7a depicts the digital photographic images of samples and Fig. 7b represents the microscopic

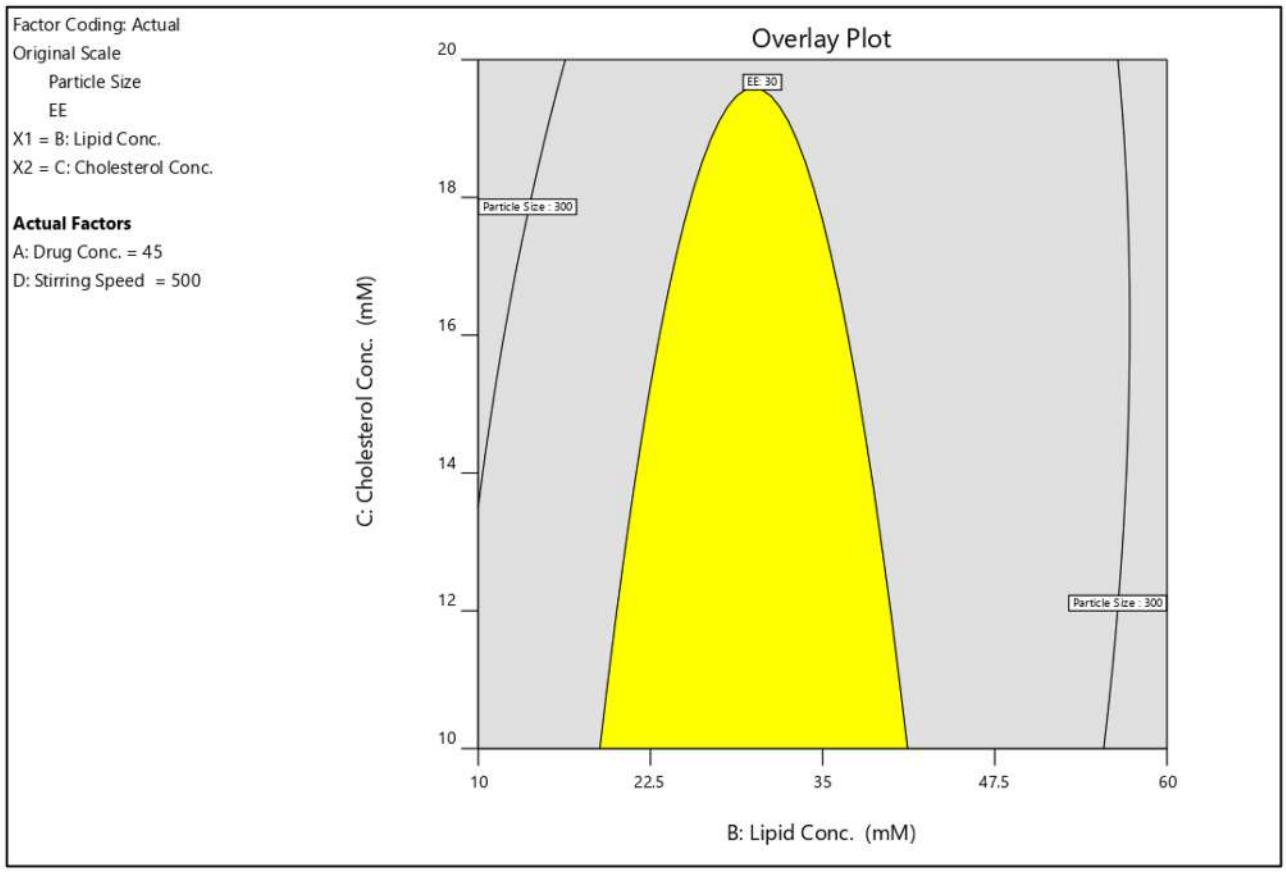

Fig. 4 Design space

images of RBCs after incubation of sample revealing absence of cell lysis.

In Vitro Drug Release Study

The release profiles obtained from the in vitro release study of developed teriparatide loaded liposomes and free teriparatide and depicted in Fig. 8. Free teriparatide showed a swift release pattern within the initial time points. The liposomal system exhibited a steady release pattern of teriparatide resulting in $54.53 \pm 0.89\%$ release in 24 h. It took 36 h to reach a maximum release of $94.95 \pm 0.62\%$ and hence, a sustained release of the drug could be observed.

As a part of predicting the drug release kinetics, the best model is decided as the one having highest $R^2_{adjusted}$ value and smallest AIC value. Furthermore, the model is appropriate when MSC value (modified reciprocal form of AIC) is greater than 2 or 3 [37]. Figure 9 represents the graphs showing different kinetic models.

The model parameters as described in Table 8 shows that Higuchi model is the best fit model explaining the release of drug from the formulation.

In Vitro Cell Line Study

AlamarBlue assay was carried out on NIH 3T3 cell line and percent viability was calculated as shown in Fig. 10. The results were indicative of viability $\geq 89.91\%$ for all the concentrations of teriparatide formulation and $\geq 87.76\%$ for all plain drug concentrations. No significant cell death was observed after the administration of formulations.

Table 7 Batches for model validation

Input variables and Responses	Unit	Batch		
		1	2	3
A: Drug conc	μM	57.49	41.25	44.59
B: Lipid conc	mM	30.70	36.40	21.76
C: Cholesterol conc	mM	13.45	11.34	13.78
D: Stirring speed	rpm	540.42	317.32	547.15
Predicted EE	%	31.31	31.31	31.31
Observed EE	%	31.79	30.41	30.01
Predicted particle size	nm	174.02	183.99	204.70
Observed particle size	nm	177.60	187.20	208.90

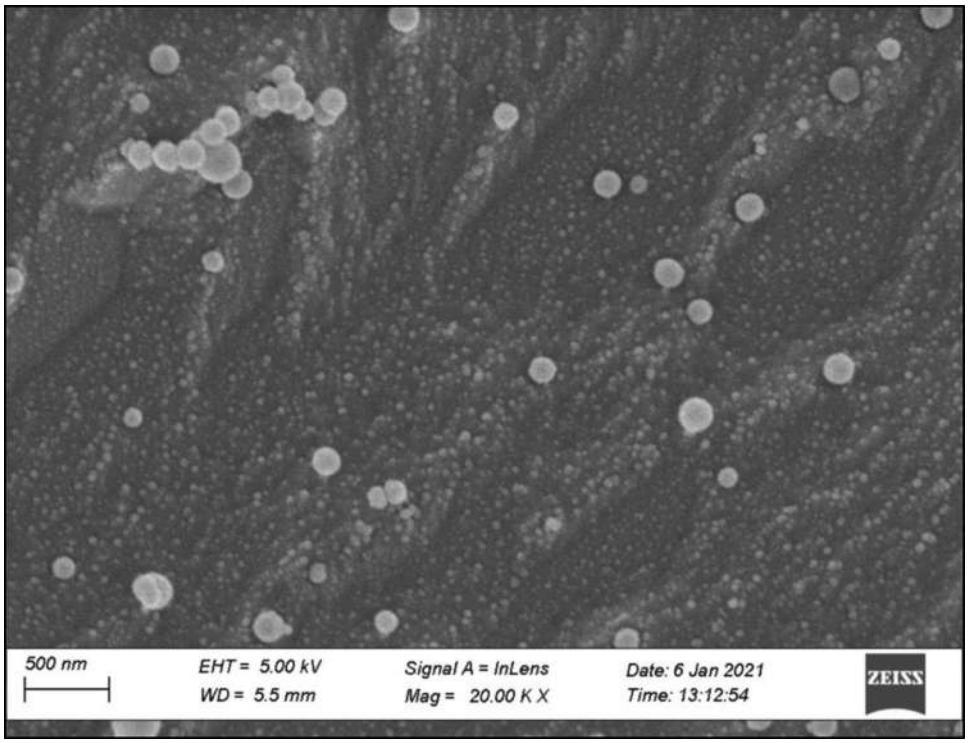

Fig. 5 Cryo FE-SEM image of optimized liposomes

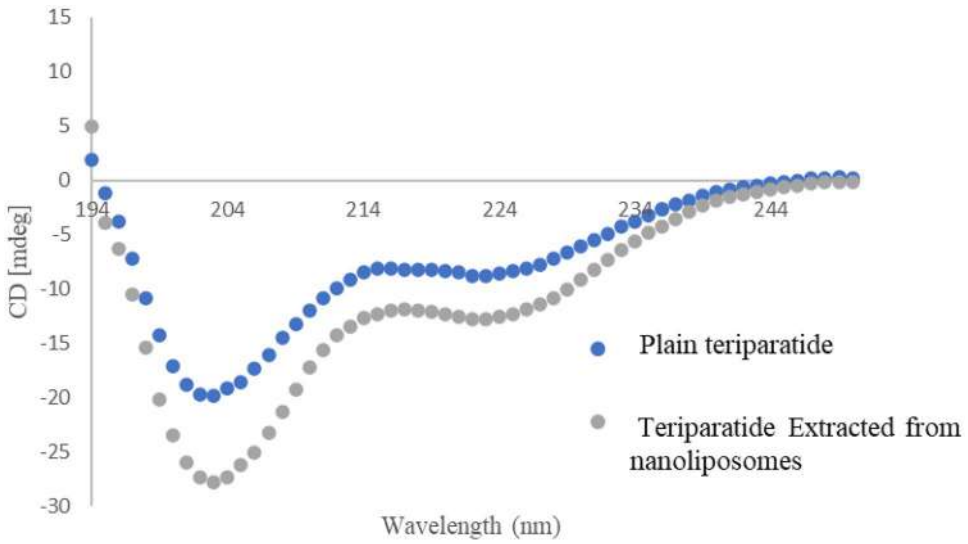

Fig. 6 Circular dichroism spectra of pure teriparatide and processed teriparatide

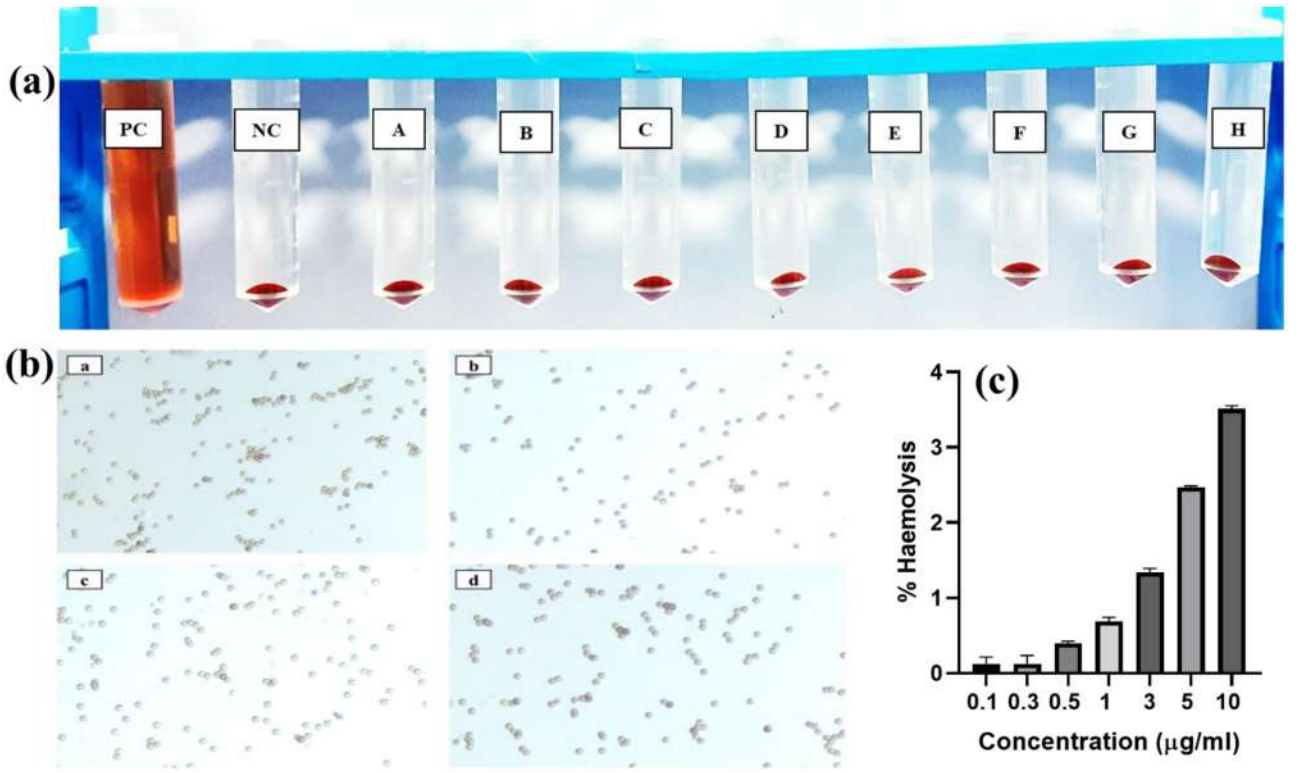

Fig. 7 **a** Images of RBCs treated with formulation of various concentrations: PC, positive control; NC, negative control; A, 0.1 μg/ml; B, 0.3 μg/ml; C, 0.5 μg/ml; D, 1 μg/ml; E, 3 μg/ml; F, 5 μg/ml; G, 10 μg/ml (**b**). Representative optical microscopic images of RBCs after incubation with different concentration; a, negative control; b, 0.1 μg/ml; c, 5 μg/ml; d, 10 μg/ml (**c**). Percentage haemolysis of various concentration of liposomes

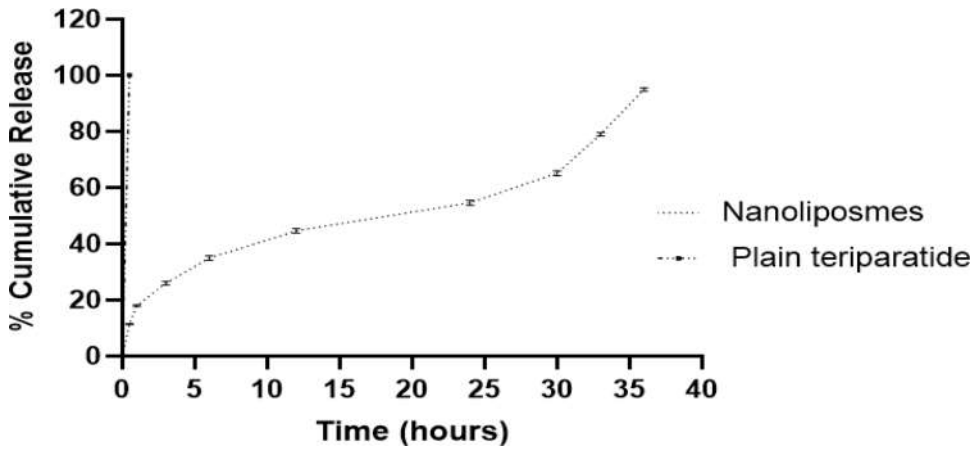

Fig. 8 In vitro release profile of free teriparatide and teriparatide-loaded liposomes ($n=3$)

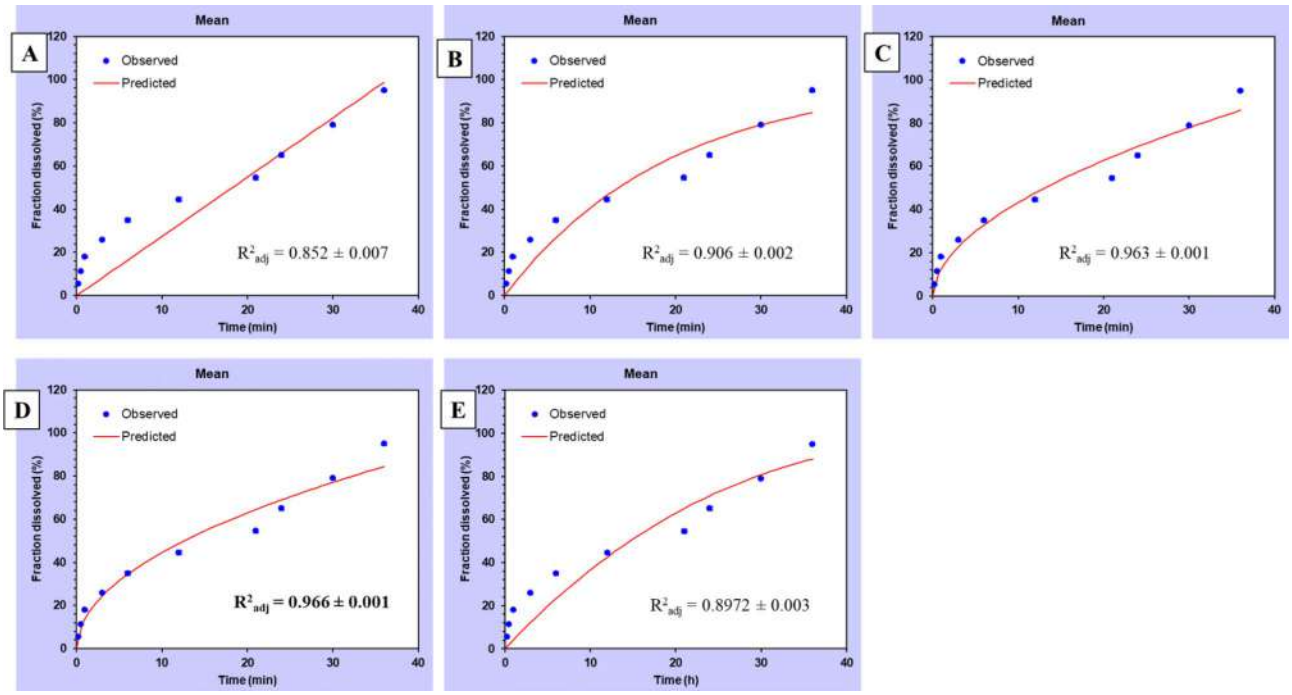

Fig. 9 The observed and predicted values of drug release presented together with model prediction using **A** zero order, **B** first order, **C** Korsmeyer-Peppas, **D** Higuchi, and **E** Hixson-Crowell

Table 8 Statistical parameters of models to describe the drug release from the formulation

Model	Statistical parameters of models (mean ± SD)		
	$R^2_{adjusted}$	AIC	MSC
Zero order	0.852 ± 0.007	72.72 ± 0.595	1.715 ± 0.051
First order	0.906 ± 0.002	68.20 ± 0.264	2.168 ± 0.022
Korsmeyer-Peppas	0.963 ± 0.001	59.50 ± 0.328	3.038 ± 0.042
Higuchi	**0.966 ± 0.001**	**57.95 ± 0.478**	**3.193 ± 0.057**
Hixson-Crowell	0.8972 ± 0.003	69.12 ± 0.389	2.075 ± 0.033

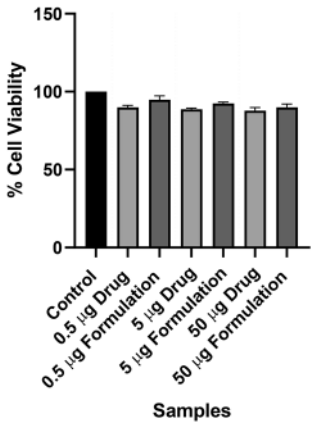

Fig. 10 Percent cell viability following AlamarBlue assay ($n = 3$)

Conclusions

Osteoporosis, a systemic skeletal disease, is characterized by increased bone fragility and loss of bone density. The endogenous PTH when acts anabolically promotes bone formation and bone remodeling. Teriparatide (human recombinant PTH peptide 1–34) is the only peptide-based anabolic drug available across the globe which enhances bone formation. However, it has a very short half-life and therefore, currently, it is administered as daily subcutaneous injection and this mode of administration leads to poor patient compliance. Liposomes can be tuned to efficiently encapsulate both hydrophobic as well as hydrophilic drugs. Teriparatide being a water-soluble peptide drug generally poses a problem in achieving high drug loading. Therefore, we developed teriparatide-loaded vesicular system to enable the sustained release of encapsulated drug. Ethanol injection technique was employed to produce monodispersed liposomes eliminating the requirement for sonication or extrusion as in the thin-film hydration method. Preliminary studies were performed to screen out CPP and CMA. The systematic approach of QbD was employed for a sound understanding of process and product control and quality risk management. Leveraging Design Expert software, Box–Behnken three-level fractionate factorial matrix design, was employed for optimization of the formulation. The developed liposomal formulation of teriparatide was

characterized for particle size (186.9 ± 2.20 nm) and polydispersity index (0.149 ± 0.02) by Zetasizer. The surface morphology was observed by cryo FE-SEM and %EE (46.52%) by HPLC. Circular dichroism spectra of encapsulated teriparatide were obtained, concluding intact secondary structure of the drug. Haemolysis assay showed absence of RBC lysis up to 10 µg/ml concentration of the formulation. The optimized formulation was subjected to an in vitro drug release study and a prolonged release profile up to 36 h was obtained. The drug release data were fitted to different release kinetics models and the release of teriparatide from the developed formulation followed Higuchi model. As a part of the in vitro cell line study, alamarBlue assay was carried out on NIH 3T3 cell line and > 87% cell viability was obtained. The liposomal formulation of teriparatide was successfully designed and optimized. The sustained release of teriparatide from the developed liposomal formulation holds the potential for increasing the half-life of teriparatide and therefore would decrease the frequency of administration, improving the patient compliance. In accordance with the anticipated outcomes attained in this work, the projected system could further be evaluated for in vivo pharmacokinetics and efficacy studies. By modifying these liposomes, target delivery can be achieved, eliminating the off-target effects of the drug for effectively treating the osteoporosis.

Declarations

Conflict of Interest The authors declare no competing of interests.

References

1. Langdahl B, Ferrari S, Dempster DW. Bone modeling and remodeling: potential as therapeutic targets for the treatment of osteoporosis. Ther Adv Musculoskelet Dis. 2016;8(6):225. https://doi.org/10.1177/1759720X16670154.
2. Blake GM, Fogelman I. The role of DXA bone density scans in the diagnosis and treatment of osteoporosis. Postgrad Med J. 2007;83:509–17. https://doi.org/10.1136/pgmj.2007.057505.
3. Wei H, Xu Y, Wang Y, Xu L, Mo C, Li L, et al. Identification of fibroblast activation protein as an osteogenic suppressor and anti-osteoporosis drug target. Cell Rep. 2020;33(2): 108252. https://doi.org/10.1016/j.celrep.2020.108252.
4. Sozen T, Ozisik L, Calik BN. An overview and management of osteoporosis. Eur J Rheumatol. 2017;4(1):46–56. https://doi.org/10.5152/eurjrheum.2016.048.
5. Föger-Samwald U, Dovjak P, Azizi-Semrad U, Kerschan-Schindl K, Pietschmann P. Osteoporosis: Pathophysiology and therapeutic options. Excli J. 2020;19:1017–37. https://doi.org/10.17179/excli2020-2591.
6. Chen JS, Sambrook PN. Antiresorptive therapies for osteoporosis: a clinical overview. Nat Rev Endocrinol. 2012;8(2):81–91. https://doi.org/10.1038/nrendo.2011.146.
7. Quattrocchi E, Kourlas H. Teriparatide: a review. Clin Ther. 2004;26(6):841–54. https://doi.org/10.1016/S0149-2918(04)90128-2.
8. Salave S, Rana D, Benival D. Peptide functionalised nanocarriers for bone specific delivery of PTH (1–34) in osteoporosis. Curr Nanomedicine. 2021;11:142–8. https://doi.org/10.2174/2468187312666211220112324.
9. Estell EG, Rosen CJ. Emerging insights into the comparative effectiveness of anabolic therapies for osteoporosis. Nat Rev Endocrinol. 2021;17(1):31–46. https://doi.org/10.1038/s41574-020-00426-5.
10. Lane NE, Kelman A. A review of anabolic therapies for osteoporosis. Arthritis Res Ther. 2003;5(5):214–22. https://doi.org/10.1186/ar797.
11. Mahajan A, Narayanan M, Jaffers G, Concepcion L. Hypoparathyroidism associated with severe mineral bone disease postrenal transplantation, treated successfully with recombinant PTH. Hemodial Int. 2009;13(4):547–50. https://doi.org/10.1111/j.1542-4758.2009.00380.x.
12. FORTEO (teriparatide) Label. 2020. https://www.accessdata.fda.gov/drugsatfda_docs/label/2020/021318s053lbl.pdf. Accessed 01 Apr 2022.
13. Application to extend duration of treatment for Teribone™ osteoporosis drug. https://www.asahi-kasei.com/news/2016/e160722.html. Accessed 01 Apr 2022.
14. Approval to manufacture and sell Teribone™ autoinjector. 2019. https://www.asahi-kasei.com/news/2019/e190920_2.html. Accessed 01 Apr 2022.
15. Sugimoto T, Shiraki M, Fukunaga M, Kishimoto H, Hagino H, Sone T, et al. Study of twice-weekly injections of teriparatide by comparing efficacy with once-weekly injections in osteoporosis patients: the TWICE study. Osteoporos Int. 2019;30(11):2321–31. https://doi.org/10.1007/S00198-019-05111-6.
16. Kostenuik PJ, Ferrari S, Pierroz D, Bouxsein M, Morony S, Warmington KS, et al. Infrequent delivery of a long-acting PTH-Fc fusion protein has potent anabolic effects on cortical and cancellous bone. J Bone Miner Res. 2007;22(10):1534–47. https://doi.org/10.1359/JBMR.070616.
17. Rana D, Salave S, Longare S, Agarwal R, Kalia K, Benival D. Nanotherapeutics in tumour microenvironment for cancer therapy. Nanosci Nanotechnology-Asia. 2021;12. https://doi.org/10.2174/2210681211666210908144839.
18. Salave S, Rana D, Pardhe R, Bule P, Benival D. Unravelling micro and nano vesicular system in intranasal drug delivery for epilepsy. Pharm Nanotechnol. 2022;10. https://doi.org/10.2174/2211738510666220426115340.
19. Shah S, Dhawan V, Holm R, Nagarsenker MS, Perrie Y. Liposomes: advancements and innovation in the manufacturing process. Adv Drug Deliv Rev. 2020;154–155:102–22. https://doi.org/10.1016/J.ADDR.2020.07.002.
20. Barbălată CI, Tomuță I, Achim M, Boșca AB, Chereches G, Soriță O, et al. Application of the QbD approach in the development of a liposomal formulation with EGCG. J Pharm Innov. 2021;2021:1–14. https://doi.org/10.1007/S12247-021-09541-W.
21. Layek B, Mukherjee B. Tamoxifen citrate encapsulated sustained release liposomes: preparation and evaluation of physicochemical properties. Sci Pharm. 2010;78:507–15. https://doi.org/10.3797/SCIPHARM.0911-11.
22. Karumanchi DK, Skrypai Y, Thomas A, Gaillard ER. Rational design of liposomes for sustained release drug delivery of bevacizumab to treat ocular angiogenesis. J Drug Deliv Sci Technol. 2018;47:275–82. https://doi.org/10.1016/J.JDDST.2018.07.003.
23. Sun X, Wei J, Lyu J, Bian T, Liu Z, Huang J, et al. Bone-targeting drug delivery system of biomineral-binding liposomes loaded with icariin enhances the treatment for osteoporosis. J Nanobiotechnology. 2019;17:10. https://doi.org/10.1186/S12951-019-0447-5.
24. Assil KK, Weinreb RN. Multivesicular liposomes: sustained release of the antimetabolite cytarabine in the eye. Arch Ophthalmol. 1987;105:400–3. https://doi.org/10.1001/ARCHOPHT.1987.01060030120040.
25. DepoDur ® (morphine sulfate extended-release liposome injection) 2007. https://www.accessdata.fda.gov/drugsatfda_docs/label/2007/021671s019lbl.pdf. Accessed 11 May 2022.

26. Hartrick CT, Hartrick KA. Extended-release epidural morphine (DepoDur): review and safety analysis. Expert Rev Neurother. 2008;8:1641–8. https://doi.org/10.1586/14737175.8.11.1641.
27. FDA. Liposome Drug Products: Chemistry, Manufacturing, and Controls; Human Pharmacokinetics and Bioavailability; and Labeling Documentation. Guidance for Industry. 2018;(August):1–15.
28. ICH. Ich Harmonised Tripartite Guideline, Pharmaceutical Development Q8(R2). ICH Harmon Tripart Guidel. 2009;8(August):1–28.
29. Porfire A, Achim M, Barbalata C, Rus I, Tomuta I, Cristea C. Pharmaceutical development of liposomes using the QbD approach. Liposomes - Adv Perspect. 2019. https://doi.org/10.5772/intechopen.85374.
30. Bhattacharyya S, Sogali BS. Application of statistical design to assess the critical process parameters of ethanol injection method for the preparation of liposomes. Dhaka Univ J Pharm Sci. 2019;18(1):103–11. https://doi.org/10.3329/dujps.v18i1.41897.
31. Shaker S, Gardouh A, Ghorab M. Factors affecting liposomes particle size prepared by ethanol injection method. Res Pharm Sci. 2017;12(5):346–52. https://doi.org/10.4103/1735-5362.213979.
32. Bahari Javan N, Rezaie Shirmard L, Jafary Omid N, Akbari Javar H, Rafiee Tehrani M, Abedin DF. Preparation, statistical optimisation and in vitro characterisation of poly (3-hydroxybutyrate-co-3-hydroxyvalerate)/poly (lactic-co-glycolic acid) blend nanoparticles for prolonged delivery of teriparatide. J Microencapsul. 2016;33(5):460–74. https://doi.org/10.1080/02652048.2016.1208296.
33. Neves AR, Lúcio M, Martins S, Lima JLC, Reis S. Novel resveratrol nanodelivery systems based on lipid nanoparticles to enhance its oral bioavailability. Int J Nanomedicine. 2013;8:177–87. https://doi.org/10.2147/IJN.S37840.
34. Goyanes A, Chang H, Sedough D, Hatton GB, Wang J, Buanz A, et al. Fabrication of controlled-release budesonide tablets via desktop (FDM) 3D printing. Int J Pharm. 2015;496(2):414–20. https://doi.org/10.1016/j.ijpharm.2015.10.039.
35. Narayanan D, Anitha A, Jayakumar R, Chennazhi KP. PTH 1–34 loaded thiolated chitosan nanoparticles for osteoporosis: oral bioavailability and anabolic effect on primary osteoblast cells. J Biomed Nanotechnol. 2014;10(1):166–78. https://doi.org/10.1166/jbn.2014.1700.
36. Baskaran R, Lee CJ, Kang SM, Oh Y, Jin SE, Lee DH, et al. Poly(lactic-co-glycolic acid) microspheres containing a recombinant parathyroid hormone (1–34) for sustained release in a rat model. Indian J Pharm Sci. 2018;80(5):837–43. https://doi.org/10.4172/pharmaceutical-sciences.1000429.
37. Siswanto A, Fudholi A, Nugroho AK, et al. In vitro release modeling of aspirin floating tablets using DDSolver. Indones. J Pharm. 2015:4;26(2):94. https://doi.org/10.14499/indonesianjpharm26iss2pp94.
38. Altaani BM, Almaaytah AM, Dadou S, Alkhamis K, Daradka MH, Hananeh W. Oral delivery of teriparatide using a nanoemulsion system: design, in vitro and in vivo evaluation. Pharm Res. 2020;37(4):80. https://doi.org/10.1007/s11095-020-02793-0.
39. Pallagi E, Jójárt-Laczkovich O, Németh Z, Szabó-Révész P, Csóka I. Application of the QbD-based approach in the early development of liposomes for nasal administration. Int J Pharm. 2019;562:11–22. https://doi.org/10.1016/j.ijpharm.2019.03.021.
40. Fukuda IM, Pinto CFF, Moreira CDS, Saviano AM, Lourenço FR. Design of experiments (DoE) applied to pharmaceutical and analytical quality by design (QbD). Brazilian J Pharm Sci. 2018;54. https://doi.org/10.1590/s2175-97902018000001006.
41. Amani N, Javar HA, Dorkoosh FA, Rouini MR, Amini M, Sharifzadeh M, et al. Preparation and pulsatile release evaluation of teriparatide-loaded multilayer implant composed of polyanhydride-hydrogel layers using spin coating for the treatment of osteoporosis. J Pharm Innov. 2020;1(3)–22. https://doi.org/10.1007/s12247-020-09453-1.